minerals

MDPI

Article

Petrogenesis of the Early Cretaceous Zhouguan Granodiorite in Jiaodong Peninsula: Evidence from Mineralogy, Geochemistry, Geochronology, and Sr-Nd Isotopes

Naijie Chi [1,2,*], Zuozhen Han [1,*], Ruicong Tian [2], Chuan'e Liu [3], Wei Shan [2], Yuqiang Xiong [4], Zengsheng Li [2], Yufeng Xie [1,5], Min Li [2] and Xiufeng Wang [2]

1 College of Earth Science and Engineering, Shandong University of Science and Technology, Qingdao 266590, China; xyfs0512@163.com
2 Key Laboratonry of Gold Mineralization Processes and Resource Utilization, MNR, Shandong Provincial Key Laboratory of Metallogenic Geological Process and Resource Utilization, Shandong Institute of Geological Sciences, Jinan 250013, China; tommyclerk88@gmail.com (R.T.); shanwei8801@163.com (W.S.); lizengsheng@126.com (Z.L.); a464850665@126.com (M.L.); xfeng68@126.com (X.W.)
3 Shandong Provincial Geo-Mineral Engineeriing Exploration Institute, Jinan 250014, China; smart668@126.com
4 Shandong Geological Exploration Insititute of China Chemical Geological and Mine Bureau, Jinan 250015, China; xiongyuqiang@163.com
5 Weifang Architectural Design and Research Institute Co., Ltd., Weifang 261022, China
* Correspondence: chinaijie@163.com (N.C.); hanzzs@163.com (Z.H.)

Abstract: The Jiaodong Peninsula is the most important gold mineralization area in China, and the formation of gold deposits is closely related to granitoids. The isotopic ages of the Early Cretaceous granodiorites in the northwestern Jiaodong Peninsula are concentrated in the range of 111~123 Ma, and are coeval with the formation of the gold deposits in the area. However, the studies on the geotectonic settings of the granodiorites, especially their petrogenesis and relationship with gold deposits in the northwestern Jiaodong Peninsula, are scarce. Based on field and petrographic observations, geochemistry, EPMA analysis, zircon U-Pb chronology, and Sr-Nd isotopes of the Early Cretaceous Zhouguan granodiorite in the Jiaodong area, the formation age of Zhouguan granodiorite is determined as 115 Ma ± 0.77 Ma; the analysis of EPMA shows that biotite is mainly composed of Fe-biotite and Mg-biotite, with its MgO content ranging from 9.797% to 11.635%. The crystallization temperature of biotite is in the range of 500 °C~625 °C and the emplacement depth of the rock mass is 3.98~8.71 km. The amphibole in the mass mainly includes magnesiohornblende, pargasite, and magnesiosadanagaite; among them, the former two are of crustal origin, while magnesiosadanagaite is of mantle origin. The crystallization pressure and depth of the former two are in the range of 0.75~3.02 kbar and 2.81~11.4 km, respectively, while the crystallization pressure and depth for the latter is 4.64 kbar and 17.53 km, respectively. The ($^{87}Sr/^{86}Sr$) values range from 0.710424 to 0.711074 and the ($^{143}Nd/^{144}Nd$) values range from 0.511530 to 0.511808. The parental magma of the Zhouguan granodiorite is highly oxidized with high-water content that is favorable for Au enrichment. Combined with the Nb-Y and Yb-Ta diagrams, a model describing the formation of Zhouguan granodiorite is proposed.

Keywords: Zhouguan granodiorite; biotite; amphibole; zircon U-Pb dating; Sr-Nd isotope; petrogenesis; Jiaodong

Citation: Chi, N.; Han, Z.; Tian, R.; Liu, C.; Shan, W.; Xiong, Y.; Li, Z.; Xie, Y.; Li, M.; Wang, X. Petrogenesis of the Early Cretaceous Zhouguan Granodiorite in Jiaodong Peninsula: Evidence from Mineralogy, Geochemistry, Geochronology, and Sr-Nd Isotopes. *Minerals* **2022**, *12*, 962. https://doi.org/10.3390/min12080962

Academic Editors: Jaroslav Dostal, Kunfeng Qiu and Callum Hetherington

Received: 12 May 2022
Accepted: 21 July 2022
Published: 29 July 2022

1. Introduction

The Jiaodong area is the largest gold producer in China, with more than 5000 t of proven gold resources [1–4]. Some large gold deposits in China such as the Sanshandao, the Jiaojia, and the Linglong gold deposits are all distributed here. The metallogenic age of the Jiaodong gold deposits is the late of the Early Cretaceous, and they have a spatial and temporal relationship with widely distributed intermediate-acid magmatic rock. The origin

and evolution process of magmas is of great significance for a correct understanding of the lithospheric structure, large-scale lithospheric thinning, and regional gold mineralization in the Jiaodong area.

Geologists researched the relationship in genesis and spatiotemporal distribution between gold deposits, Mesozoic magmatic rocks, and basic dykes in the Jiaodong area, which led to three main view points: (1) the formation of gold deposits is related to the Late Jurassic Linglong granite (160–150 Ma) and the Early Cretaceous Guojialing granodiorite (130–126 Ma) [5–10]; (2) the formation of gold deposits is closely related to the late of the Early Cretaceous Weideshan granodiorite (120–100 Ma) [11–17], and the Zhouguan granodiorite studied in this paper is comparable to the Weideshan granodiorite; (3) the formation of gold deposits is related to the contemporaneous basic intrusive rocks, the source materials of which come from the enriched lithospheric mantle [18–27].

Many studies on Mesozoic intrusive rocks in the Jiaodong area are mainly focused on petrology, geochronology, element, and isotopic geochemistry, etc., but there are relatively few studies on the physical and chemical conditions of magma crystallization [28–33]. The changes in physical and chemical conditions during different stages of magmatic evolution are still unclear, which affects the evaluation of the potential of mineralization and diagenesis of the Mesozoic granitoids. The physical and chemical conditions (pressure, temperature, oxygen fugacity, etc.) during the formation of granites directly affect the distribution of ore-forming elements, which, in turn, shape ore-forming and granitic magma evolution [34,35]. The chemical study of biotite and amphibole can effectively reflect the changing physical and chemical conditions of the petrogenetic process, and provide information on the source of petrogenetic materials, environment and mineralization, etc. [36–42]. Therefore, through further study of the single minerals in granodiorite, the physical and chemical conditions of the petrogenetic process can be determined, which can deepen the understanding of the relationship between magmatism and gold mineralization during the late of the Early Cretaceous in the Jiaodong area.

We selected the late of the Early Cretaceous representative, Zhouguan granodiorite in the northwest Jiaodong Peninsula, for a detailed field geological investigation, sampling, microscope observation, systematic study of minerals, whole-rock major and trace element geochemistry, zircon U-Pb dating, and Sr-Nd isotopes, to determine the geochemical features of the Zhouguan granodiorite that place further constraints on its formation age and petrogenesis. The tectonic environment and geological process of the northwest Jiaodong Peninsula were discussed.

2. Regional Geology

The northwest area of the Jiaodong Peninsula lies in the southeastern edge of the North China Craton (Figure 1a), to the east of the Tan-Lu fault and in the Jiaobei uplift. The terrane is composed of the metamorphic rocks of the Neoarchean Jiaodong Group, the Paleoproterozoic Jingshan and Fenzishan Groups, the Neoproterozoic Penglai Group and the Mesozoic–Cenozoic formation. Structurally, the northwest Jiaodong Peninsula has three major NNE-NE-trending faults, i.e., the Sanshandao, the Jiaojia, and the Zhaoping faults as well as the NE-trending Lingbei and Yidao faults (Figure 1b), which are considered to be subsidiaries of the Tan-Lu fault.

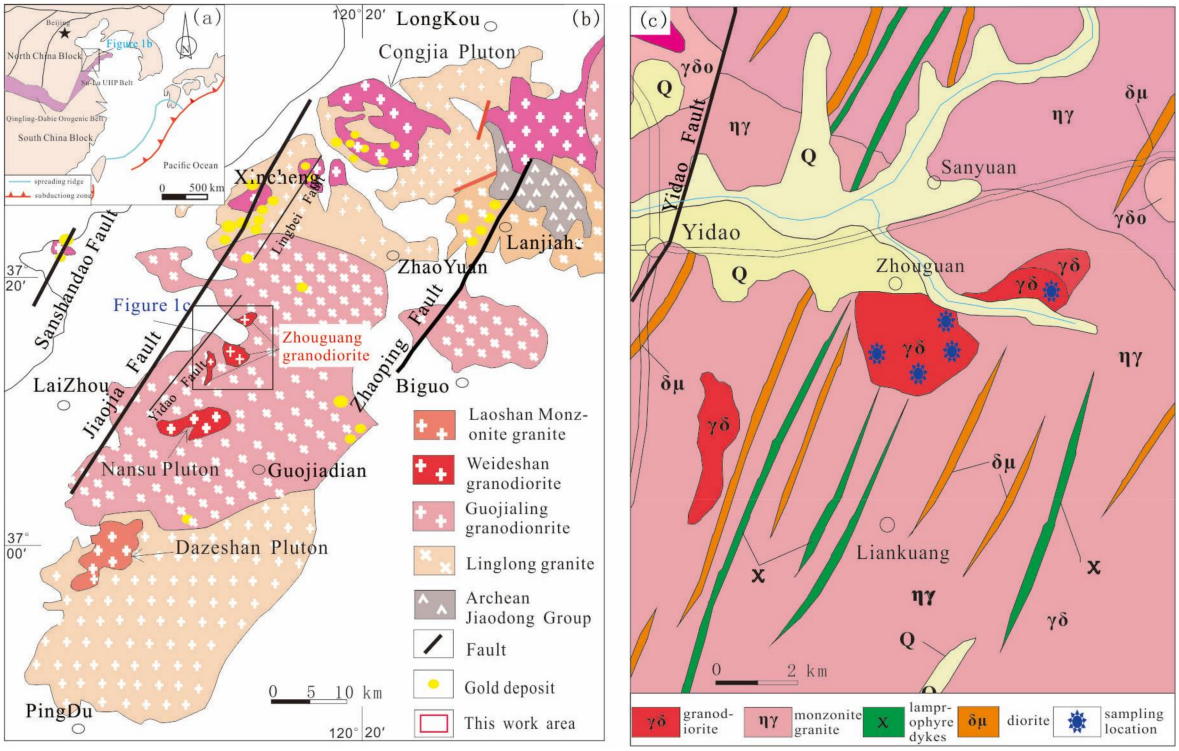

Figure 1. Simplified geologic map of the Jiaodong area. (**a**) The structure outline map, (**b**) The regional geological map of Jiaodong area (modified after Lu et al., 2011 [43]) and (**c**) The study area.

Magmatic rocks are widely distributed in the northwest Jiaodong Peninsula. They mainly include the Late Jurassic Linglong biotite two-feldspar granite with an age of 160 Ma–150 Ma, which belongs to the calc-alkaline granite formed by in situ crust remelting, the Early Cretaceous Guojialing granodiorite with an age of 130 Ma–126 Ma, which belongs to high-K calc-alkaline granodiorite of mixed crustal–mantle origin and the Early Cretaceous Weideshan granodiorite with an age of 120 Ma–100 Ma, i.e., the high-K calc-alkaline granodiorite of mixed crustal–mantle origin [44,45]. The Guojialing and the Weideshan granodiorites intruded into the Linglong granite in the NEE direction mainly along the Lingbei fault and the Yidao fault in the study area. The intrusions of the Weideshan stage in the study area mainly include the Zhouguan, the Nansu, and the Dazeshan stocks (Figure 1b). In the north and east of the Zhouguan granodiorite, a lot of gold deposits are distributed around. Compared to Guojialing granite, Nansu and Dazeshan granodiorite are more spatially and temporally significant, and the systematic study of Zhouguan granodiorite is more significant for studying the relationship between magmatism and gold mineralization. So in this study, we focused on the Zhouguan granodiorite (Figure 1c), which is located near Dongzhouguan Village, Yidao Town of Laizhou City. The rock ranges from light grey to grey-white in color, with a texture ranging from semi-hedral to medium-grained and a massive structure (Figure 2a); and is mainly composed of plagioclase (30%~40%), K-feldspar (15%~20%), quartz (25%~30%), biotite (5%~10%), amphibole (3%~4%), and opaque minerals (1%), with accessory minerals of zircon, apatite, sphene, and magnetite (Figure 2b–d). The plagioclase occurs as euhedral-to-semihedral long platy crystals with zoning. Biotite exhibits from light brown to brown pleochroism and can be replaced by chlorite or epidote, or replaced by sericite in its edge. The K-feldspar occurs as regular platy phenocrysts with zoning and a streaky structure.

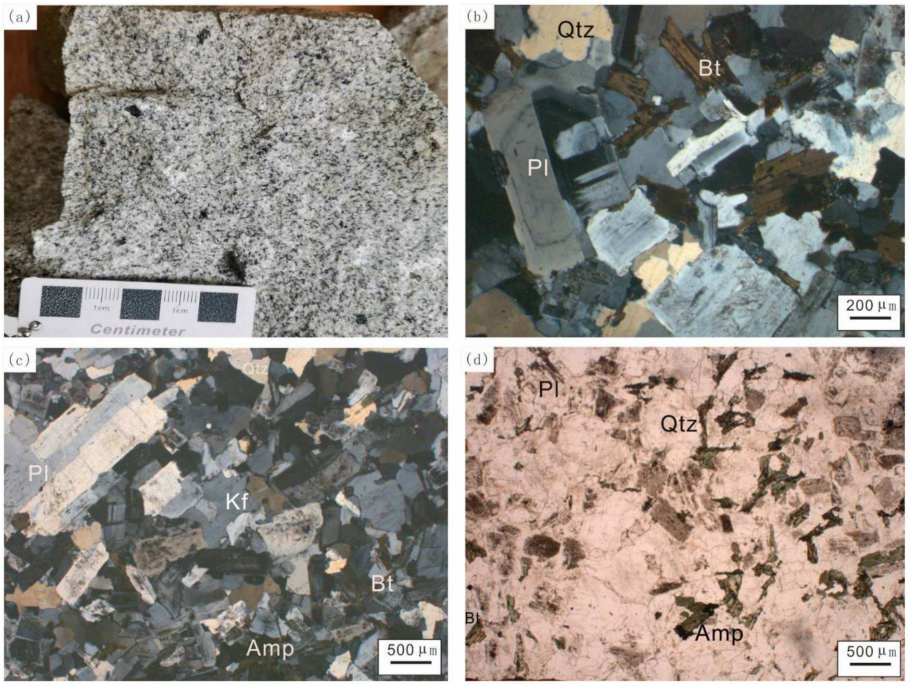

Figure 2. The petrographic characteristics of the Zhouguan granodiorite. (**a**) Granodiorite hand specimen; (**b**–**d**) photomicrographs of granodiorite showing the main rock-forming minerals of quartz (Qtz), plagioclase (Pl), K-feldspar (Kf), biotite (Bt), and amphibole (Amp).

3. Samples and Analytical Methods

3.1. Geochemical Analysis

Samples (ZG0721-b1, -b3, -b5, -b8, and –b10) were collected from Zhouguan granodiorite for geochemical analysis. The geochemical analysis was carried out in the Jinan Mineral Resources Supervision and Testing Center of the Ministry of Land and Resources. The trace elements and REE analysis were performed on the plasma emission spectrometer (ICP-AES, IRISIntrepid II), atomic absorption spectrometer (AASPE400, PE600), atomic fluorescence spectrometer (AFS-820), and plasma mass spectrometer (ICP-MS, XSERIES2) using the national standards GB/T14506-2010 "Chemical Analysis Method of Silicate Rock" for control. The operating temperature and relative humidity are 20°C and 30%, respectively. The error of major element analysis is within 1%, the accuracy of trace element content is better than 3% when the content of trace elements is greater than 10×10^{-6}, while the accuracy is better than 10% when the content of trace elements is less than 10×10^{-6} [46–48]. The data are given in Tables 1 and 2.

Table 1. Contents of major elements (%) of the Zhouguan granodiorite samples.

Liths	Granodiorite				Granite Porphyry	Guojialing Granite	Linglong Granite	Adakite	TTG		High Sr-Ba Granite
Number	ZG0721-b1	ZG0721-b3	ZG0721-b5	ZG0721-b8	ZG0721-b10	GJL-1	LL-1	AI-1 [48]	TTG-1 [48]	TTG-2 [48]	Sr-1 [48]
SiO2	68.09	68.72	68.07	68.24	73	72.26	72.74	63.89	70.2	68.53	71.14
Al2O3	15.22	15.82	15.78	16.07	14.23	14.46	12.32	17.4	15.74	15.91	15.06
Fe2O3	2.48	2.57	2.67	2.53	1.52	1.67	1.05	4.68	2.84	2.49	1.02
K2O	3.77	3.05	3.08	3.16	4.34	4.29	4.96	1.52	1.88	1.56	4.22
Na2O	4.11	4.18	4.16	4.23	3.88	3.9	4.83	4.09	4.87	5.57	4.35
CaO	2.73	2.96	2.65	2.99	1.51	1.63	2.03	5.23	3.17	3.36	1.46
MgO	1.36	1.39	1.32	1.21	0.66	0.28	0.39	2.2	1.09	1.41	0.26
TiO2	0.33	0.37	0.38	0.4	0.2	-	-	-	-	-	-
MnO	0.043	0.042	0.04	0.034	0.022	-	0.2	0.08	0.04	0.04	0.01
P2O5	0.16	0.15	0.13	0.15	0.09	0.04	0.06	0.19	0.12	0.11	0.06
LOI	1.42	0.89	1.92	0.82	0.68	0.48	0.81	-	-	-	-
Total	99.713	100.142	100.2	99.834	100.132	99.01	99.39	99.28	99.95	98.98	97.58
	Contents of Au element (ppb) of Zhouguan granodiorite										
Au	<0.5	0.8	<0.5	<0.5	<0.5	-	-	-	-	-	-

Table 2. Analysis results of trace and rare earth elements (μg/g) in the Zhouguan granodiorite.

No.	ZG0721-b1	ZG0721-b3	ZG0721-b5	ZG0721-b8	ZG0721-b10	No.	ZG0721-b1	ZG0721-b3	ZG0721-b5	ZG0721-b8	ZG0721-b10
Liths	Granodiorite				Granite Porphyry	Liths	Granodiorite				Granite Porphyry
Rb	86.6	66.4	65.5	61.1	104	Ce	68.5	56.9	54.5	70	56.6
K	31,296.61	25,319.54	25,568.58	26,232.70	36,028.46	Pr	9.09	7.4	7.13	9.14	7.09
Ba	2091	1941	2052	2116	1458	Nd	31.8	26.4	25.8	32.5	24.1
Th	14.5	9.91	9.37	12	18.9	Sm	4.77	4.08	3.94	4.81	3.57
U	2.15	1.34	1.46	1.7	2.13	Eu	1.08	0.95	0.91	1.13	0.75
Nb	7.8	6.13	5.78	6.75	8.64	Gd	4.08	3.57	3.54	4.12	3.14
La	51	40.1	38.2	50	40.9	Tb	0.45	0.38	0.38	0.42	0.35
Ce	68.5	56.9	54.5	70	56.6	Dy	1.84	1.57	1.55	1.65	1.47
Sr	900	953	928	1042	531	Ho	0.34	0.29	0.29	0.29	0.28
Nd	31.8	26.4	25.8	32.5	24.1	Er	0.94	0.78	0.78	0.78	0.81
P	698.21	654.57	567.29	654.57	392.74	Tm	0.13	0.1	0.11	0.099	0.12
Zr	154	133	136	148	115	ΣREE	175.12	143.34	138.01	175.72	140.22
Hf	4.31	3.79	4.09	4.38	3.73	LREE	166.24	135.83	130.48	167.58	133.01
Sn	0.65	0.64	0.73	0.52	0.6	HREE	8.88	7.51	7.53	8.139	7.21
Ti	1589	1742	1765	1930	939	LREE/ HREE	18.72	18.08	17.32	20.58	18.44
Y	9.98	8.13	7.69	7.78	8.5	LaN/YbN	38.51	40.51	36.05	53.52	32.96
Yb	0.95	0.71	0.76	0.67	0.89	δEu	0.75	0.76	0.74	0.77	0.68
Lu	0.15	0.11	0.12	0.11	0.15	δCe	0.78	0.81	0.81	0.81	0.81
La	51	40.1	38.2	50	40.9						

3.2. Zircon U-Pb Dating

The granodiorite sample (ZG0721-b8) was selected for Zircon U-Pb dating. Zircon crystals for U-Pb dating were separated from the Zhouguan granodiorite, whose target making, cathodoluminescence (CL) photography was performed by Langfang Chengxin Geological Service Co., Ltd. The analysis for U-Pb dating was conducted using the instrument LA-MC-ICP-MS at Jinan Mineral Resources Supervision and Testing Center of the Ministry of Land and Resources. More detailed analytical conditions and procedures are described by Song et al. (2010) [49] and Wang et al. (2012) [50].

In this study a total of 20 U-Pb dating points in the samples were analyzed. The results were corrected by the U-Th-Pb isotope content and age of the reference sample, and the common lead was corrected according to the measured ^{204}Pb. The individual data point error is 1σ, and the weighted average age error is 96% confident. Data processing was performed by the laboratory staff using Squid and Isoplot programs.

3.3. EPMA Analysis of Biotite and Amphibole

Representative biotite and amphibole from Zhouguan granodiorite were used for EPMA analysis. The EPMA analysis was completed in the Key Laboratory of Gold Mineralization Process and Resource Utilization, Ministry of Natural Resources, Shandong Institute of Geological Sciences. The instrument model was JXA-8230, the acceleration voltage for spectral analysis was 15 kV, the current was 1×10^{-8} A, and the beam spot diameter was 1~10 μm. All the standards were Canadian Astimex standards. The fresh and unaltered biotite and amphibole minerals were separated (picked up under binocular microscope) from the Zhouguan granodiorite and used for EPMA analyses, the EPMA data of biotite were calculated in units of 22 oxygen atoms and related parameters. The - Fe^{2+} and Fe^{3+} values were obtained with the calculation method of Lin Wenwei and Peng Lijun (1994) [51]. The amphibole EPMA data were calculated using Geokit software.

3.4. Sr-Nd Isotopes

Four samples of granodiorite were selected for Sr and Nd isotope ratio analysis. The whole-rock Sr-Nd isotopes were determined by thermal ionization mass spectrometry (ISOPROBE-T) at Langfang Chengxin Geological Service Co., Ltd. (Langfang, China). The 100 mg sample powders were dissolved in a HF + HNO_3 + $HClO_4$ mixture, separated using the conventional cation exchange technique with HCl as an eluent for Sr and Nd, and tested by a Thermal ionization mass spectrometer (TIMS).

The $^{87}Sr/^{86}Sr$ ratios were normalized to $^{88}Sr/^{86}Sr$ standard = 0.1194, while the $^{143}Nd/^{144}Nd$ ratios were normalized with $^{146}Nd/^{144}Nd$ standard = 0.7219 as the internal standard. The NBS987 Sr standard yielded a $^{87}Sr/^{86}Sr$ value of 0.710250 ± 7, and the JMC Nd standard gave $^{143}Nd/^{144}Nd$ value of 0.512109 ± 3.

4. Results

4.1. Characteristics of Whole-Rock Major and Trace Elements of Zhouguan Granodiorite

As shown in Table 1, the SiO_2 contents of the granodiorite range from 68.07% to 68.72%, with the Na_2O/K_2O ratios of 1.09~1.37. The total alkali contents (Na_2O + K_2O) are 7.23%~7.88%; the samples in the study area fall into the granodiorite field in the Na_2O + K_2O vs. SiO_2 (TAS) diagram (Figure 3a), and belong to high-K calc-alkaline series (Figure 3b). The differentiation index (DI) of the rock ranges from 78.31 to 80.5, while the aluminium index (A/CNK) is 1.43~1.59 which shows that the Zhouguan granodiorite belongs to peraluminous granite on the A/CNK-A/NK diagram (Figure 3c).

In the chondrite-normalized REE diagram (Figure 4a), it is shown that the ΣREE contents of the Zhouguan granodiorite are in the range of 138.01~175.72 ppm, and also shows light rare earth element (LREE) enrichment and heavy rare earth element (HREE) depletion. The $(La/Yb)_N$ ratios are in the range of 36.05~53.53 and the LREE/HREE ratios are 17.33~20.59, suggesting that a significant fractionation of light and heavy rare earth

elements occurred. The granodiorite has weak to moderately negative Eu (0.74~0.78) and δCe 0.78~0.81, with higher Sr and La contents and lower Y and Yb contents.

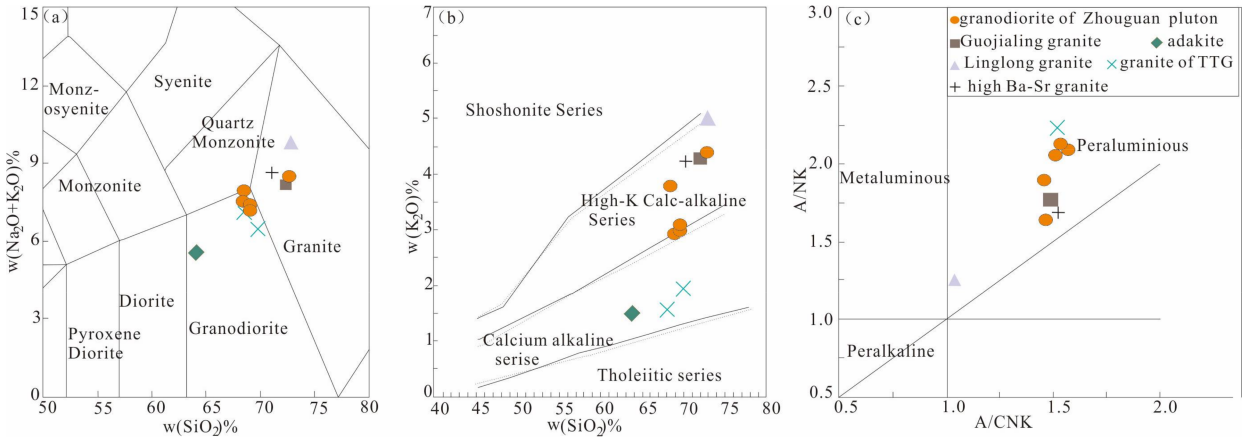

Figure 3. Variation diagram of the major elements in the Zhouguan granodiorite. (**a**) Diagram of $Na_2O + K_2O$ vs. SiO_2; (**b**) diagram of K_2O vs. SiO_2; and (**c**) diagram of A/NK vs. A/CNK.

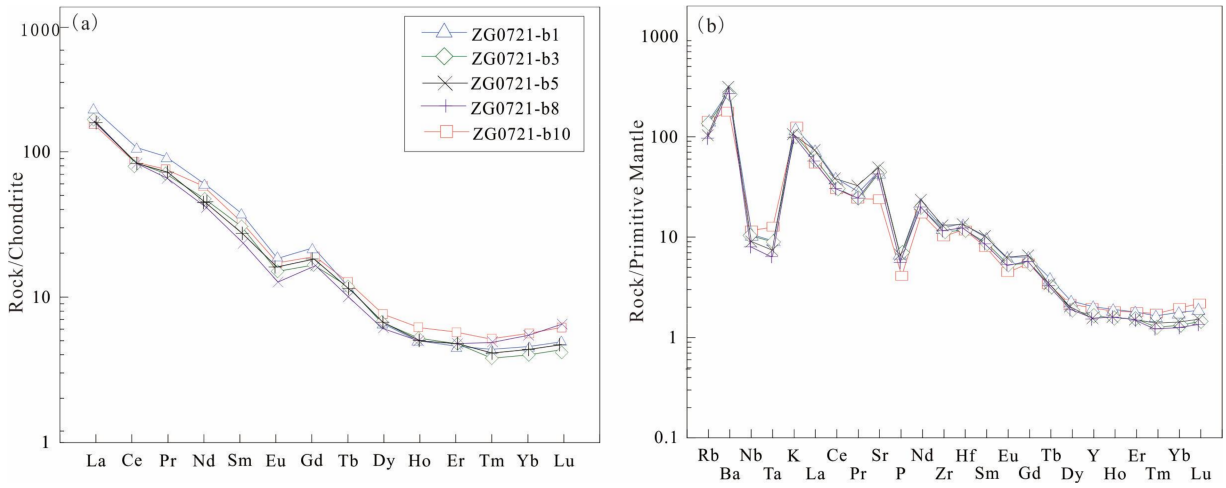

Figure 4. Chondrite-normalized rare earth elements diagram (**a**) and primitive mantle-normalized spider diagram for trace elements (**b**) of the Zhouguan granodiorite (the normalized values according to Sun and McDonough, 1989 [52]).

In the primitive mantle-normalized spider diagram (Figure 4b), the granodiorite shows the enrichment of large ion lithophile elements (LILE) such as Ba, Sr and K, and the depletion of some high field-strength elements (HFSE), such as Nb, Ta, and P, with Sr/Y ratios of 90.18~133.93.

4.2. Zircon U-Pb Age

Through LA-MC-ICP-MS zircon U-Pb dating of the Zhouguan granodiorite sample, the zircon CL images show that the zircon grains are relatively large, with its aspect ratio being 1:3~1:2. Most zircon grains show core-rim textures, with well-defined oscillatory zoning in the rim and a bright homogeneous core, which reflects its inherited growth feature and conforms to the characteristics of magmatic zircon (Figure 5).

The analysis data of U-Pb dating are shown in Table 3. The U and Th contents are in the range of 55.38~778.64 ppm and 23.14~451.5 ppm, respectively. The Th/U ratios vary from 0.92 to 1.41. Some zircon grains were spotted in both the core and rim. The age of the core varies from Precambrian through the Jurassic to Early Cretaceous, suggesting the inherited origin of some zircon grains.

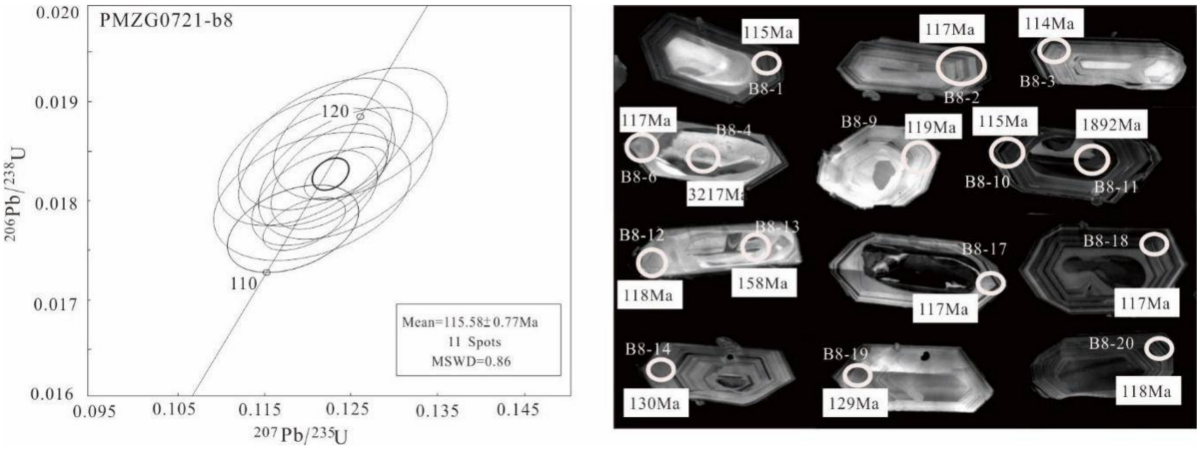

Figure 5. The CL image and the zircon U-Pb concordance diagram of zircon in the Zhouguan granodiorite.

Table 3. LA-MC-ICP-MS zircon U-Pb dating results of Zhouguan granodiorite.

No.	Pb 10^{-6}	Th 10^{-6}	U 10^{-6}	Th/U	$^{207}Pb/^{235}U$		$^{206}Pb/^{238}U$		$^{207}Pb/^{235}U$		$^{206}Pb/^{238}U$	
					Ratio	Error	Ratio	Error	Age/Ma	Error	Age/Ma	Error
B8-1	62.93	347.59	378.88	0.92	0.1192	0.0011	0.0180	0.0001	114	1.0	115	0.5
B8-2	44.96	73.82	155.15	0.48	0.1321	0.0029	0.0184	0.0001	126	2.6	117	0.9
B8-3	37.75	29.45	176.80	0.17	0.1185	0.0016	0.0178	0.0001	114	1.4	114	0.7
B8-4	1046.01	176.06	243.82	0.72	25.2427	0.2491	0.6471	0.0050	3318	9.9	3217	19.7
B8-5	31.27	129.25	121.52	1.06	0.1610	0.0032	0.0200	0.0001	152	2.8	127	0.7
B8-6	22.26	100.70	127.15	0.79	0.1201	0.0018	0.0183	0.0001	115	1.7	117	0.6
B8-7	23.85	107.41	147.50	0.73	0.1297	0.0018	0.0197	0.0001	124	1.6	125	0.7
B8-8	22.37	94.06	119.58	0.79	0.1319	0.0020	0.0196	0.0001	126	1.8	125	0.7
B8-9	40.34	206.52	180.14	1.15	0.1253	0.0016	0.0187	0.0001	120	1.5	119	0.6
B8-10	77.78	371.35	778.64	0.48	0.1201	0.0011	0.0177	0.0001	115	1.0	113	0.7
B8-11	240.50	23.14	661.91	0.03	5.4479	0.0313	0.3428	0.0018	1892	5.1	1900	8.7
B8-12	29.81	155.85	163.41	0.95	0.1226	0.0015	0.0184	0.0001	117	1.3	118	0.6
B8-13	18.42	67.82	55.38	1.22	0.1630	0.0039	0.0248	0.0002	153	3.4	158	1.3
B8-14	47.66	229.04	279.48	0.82	0.1367	0.0014	0.0204	0.0001	130	1.3	130	0.7
B8-15	26.13	85.98	282.75	0.30	0.1607	0.0016	0.0236	0.0001	151	1.4	151	0.8
B8-16	921.68	201.31	322.03	0.63	12.7009	0.0766	0.4862	0.0024	2658	6.0	2554	10.7
B8-17	15.20	66.86	64.35	1.04	0.1217	0.0030	0.0181	0.0001	117	2.7	115	0.9
B8-18	81.13	451.50	320.42	1.41	0.1226	0.0013	0.0182	0.0001	117	1.2	116	0.6
B8-19	83.12	395.23	414.09	0.95	0.1359	0.0013	0.0200	0.0001	129	1.1	128	0.7
B8-20	30.66	149.85	169.12	0.89	0.1229	0.0019	0.0183	0.0001	118	1.7	117	0.7

4.3. Biotite Analysis Results

The biotite formula is calculated on a 22 oxygen atom basis. The main characteristics of biotite in the Zhouguan granodiorite are as follows: The SiO_2 content in biotite is in the range of 34.28%~36.727% while MgO content is 9.797%~11.635% (Table 4), which means that biotite is significantly rich in Mg; the Al^{VI} + Fe^{3+} + Ti and the Fe^{2+} + Mn values are 0.316~0.556 and 1.07~1.27, respectively, with the $Fe^{2+}/(Fe^{2+} + Mg)$ ratio being 0.26~0.52. This indicates that the biotite was not subjected to late fluid alteration and belongs to primary biotite [53], which is consistent with the observation of biotite under a microscope. On the composition classification diagram of biotite (Figure 6a), both Mg-biotite and Fe-biotite are the main sub-type. The Al_2O_3 content of biotite is in the range of 13.09%~15.25% and the cation number of Al^{VI} per formula is 0.01~0.114. The high Ti and low Al^{VI} in the biotite formula indicate that the biotite was formed under the conditions of relatively high temperature and high oxygen fugacity [54,55].

Table 4. Composition of biotite in Zhouguan granodiorite.

Oxide	Samples														
	H-1	**H-2**	**H-3**	**H-4**	**H-5**	**H-6**	**H-7**	**H-8**	**H-9**	**H-10**	**H-11**	**H-12**	**H-13**	**H-14**	**H-15**
SiO_2	34.767	34.248	35.282	34.889	34.922	35.412	34.96	34.783	35.45	35.3	35.635	34.879	35.599	34.857	35.692
TiO_2	4.133	4.396	4.663	2.852	4.071	3.571	4.172	3.444	4.161	3.881	4.18	4.555	4.391	4.506	3.573
Al_2O_3	13.949	14.206	13.621	15.02	14.174	13.704	13.882	15.126	13.787	14.608	13.826	13.905	13.957	14.005	14.145
FeO	20.764	20.918	20.884	21.805	20.742	21.368	20.709	21.39	20.756	20.244	20.245	21.652	20.262	21.51	20.392
MnO	0.261	0.328	0.309	0.286	0.37	0.289	0.294	0.313	0.321	0.266	0.32	0.334	0.273	0.381	0.311
MgO	10.217	9.943	10.328	10.811	10.172	11.137	10.36	11.505	10.556	10.619	10.742	9.868	10.546	9.833	11.189
CaO	0.174	0.051	0.014	0.066	0.071	0.017	0.164	0.641	0.258	0.025	0.126	0.221	0.049	0.046	0.065
Na_2O	0.146	0.225	0.194	0.159	0.104	0.096	0.333	0.169	0.121	0.061	0.283	0.119	0.203	0.21	0.05
K_2O	9.147	9.453	8.685	8.106	9.404	8.547	9.232	6.838	8.759	9.249	8.961	8.788	9.037	8.941	8.881
Si	2.7436	2.7079	2.7618	2.7293	2.7434	2.7684	2.7441	2.6943	2.7679	2.7493	2.7733	2.7356	2.7696	2.7353	2.7737
Al^{IV}	1.2564	1.2921	1.2382	1.2707	1.2566	1.2316	1.2559	1.3057	1.2321	1.2507	1.2267	1.2644	1.2304	1.2647	1.2263
Al^{VI}	0.0409	0.0317	0.0184	0.1142	0.0556	0.0311	0.0284	0.0753	0.0366	0.0902	0.0414	0.0209	0.0493	0.0305	0.0693
Ti	0.2454	0.2615	0.2746	0.1678	0.2406	0.2100	0.2464	0.2007	0.2444	0.2274	0.2447	0.2688	0.2570	0.2660	0.2089
Fe^{3+}	0.1660	0.1373	0.2163	0.1731	0.1610	0.1763	0.1451	0.2349	0.2013	0.1831	0.1859	0.1983	0.2027	0.1854	0.1864
Fe^{2+}	1.2043	1.2459	1.1508	1.2535	1.2018	1.2208	1.2144	1.1507	1.1540	1.1355	1.1318	1.2219	1.1157	1.2262	1.1389
Mn	0.0174	0.0220	0.0205	0.0190	0.0246	0.0191	0.0195	0.0205	0.0212	0.0175	0.0211	0.0222	0.0180	0.0253	0.0205
Mg	1.2019	1.1720	1.2052	1.2608	1.1912	1.2980	1.2123	1.3286	1.2287	1.2329	1.2463	1.1538	1.2231	1.1503	1.2963
Ca	0.0147	0.0043	0.0012	0.0055	0.0060	0.0014	0.0138	0.0532	0.0216	0.0021	0.0105	0.0186	0.0041	0.0039	0.0054
Na	0.0223	0.0345	0.0294	0.0241	0.0158	0.0146	0.0507	0.0254	0.0183	0.0092	0.0427	0.0181	0.0306	0.0320	0.0075
K	0.9209	0.9535	0.8673	0.8090	0.9424	0.8524	0.9245	0.6757	0.8725	0.9190	0.8897	0.8793	0.8969	0.8951	0.8805
Total	7.8340	7.8627	7.7837	7.8269	7.8390	7.8237	7.8549	7.7651	7.7987	7.8169	7.8141	7.8017	7.7973	7.8146	7.8136
OH^-	2.0000	2.0000	2.0000	2.0000	2.0000	2.0000	2.0000	2.0000	2.0000	2.0000	2.0000	2.0000	2.0000	2.0000	2.0000
MF	0.4641	0.4548	0.4648	0.4659	0.4620	0.4782	0.4678	0.4858	0.4716	0.4799	0.4821	0.4444	0.4779	0.4446	0.4906
$Al^{VI} + Fe^{3+} + Ti$	0.4523	0.4305	0.5093	0.4551	0.4572	0.4174	0.4198	0.5109	0.4824	0.5007	0.4721	0.4879	0.5089	0.4819	0.4645
$Fe^{2+} + Mn$	1.2218	1.2679	1.1713	1.2725	1.2264	1.2399	1.2339	1.1713	1.1753	1.1531	1.1528	1.2441	1.1337	1.2516	1.1594
Ti/(Mg + Fe + Ti + Mn)	0.0865	0.0921	0.0958	0.0584	0.0853	0.0718	0.0868	0.0684	0.0858	0.0813	0.0865	0.0938	0.0913	0.0932	0.0733
Al/(Al + Mg + Fe + Ti + Mn + Si)	0.1883	0.1926	0.1825	0.1980	0.1907	0.1815	0.1867	0.1955	0.1837	0.1946	0.1843	0.1862	0.1863	0.1881	0.1871

Table 4. *Cont.*

Oxide	Samples														
	H-16	**H-17**	**H-18**	**H-19**	**H-20**	**H-21**	**H-22**	**H-23**	**H-24**	**H-25**	**H-26**	**H-27**	**H-28**	**H-29**	**H-30**
SiO_2	35.128	36.675	36.23	35.187	35.242	35.758	35.362	36.126	35.67	35.042	35.502	35.482	35.629	35.308	35.188
TiO_2	4.398	3.539	3.077	4.027	4.395	4.032	3.381	4.355	4.344	4.63	4.369	4.355	4.22	4.116	4.738
Al_2O_3	14.032	13.498	13.091	14.349	14.139	13.338	14.873	13.669	14.463	14.079	13.86	14.279	14.129	14.678	14.189
FeO	21.127	19.473	20.494	20.651	21.249	21.205	21.19	20.596	20.686	21.042	21.232	20.856	20.73	20.857	20.736
MnO	0.252	0.297	0.324	0.3	0.275	0.286	0.336	0.298	0.261	0.363	0.251	0.321	0.327	0.292	0.258
MgO	9.865	11.635	11.465	10.701	10.232	10.739	10.533	10.69	10.188	10.058	10.302	10.249	10.736	10.121	10.365
CaO	0.031	0.329	0.188	0.12	0.017	0	0.092	0	0.076	0.098	0.078	0.02	0.086	0.003	0
Na_2O	0.077	0.117	0.41	0.107	0.096	0.222	0.091	0.126	0.095	0.531	0.186	0.113	0.077	0.116	0.088
K_2O	9.509	8.872	9.25	9.087	9.01	9.152	8.927	8.876	9.02	9.032	9.026	9.229	8.967	9.446	9.435
Si	2.7514	2.8302	2.8217	2.7391	2.7453	2.7857	2.7452	2.7952	2.7616	2.7295	2.7613	2.7531	2.7582	2.7414	2.7315
Al^{IV}	1.2486	1.1698	1.1783	1.2609	1.2547	1.2143	1.2548	1.2048	1.2384	1.2705	1.2387	1.2469	1.2418	1.2586	1.2685
Al^{VI}	0.0467	0.0578	0.0233	0.0556	0.0434	0.0103	0.1060	0.0417	0.0813	0.0220	0.0318	0.0588	0.0474	0.0845	0.0296
Ti	0.2592	0.2055	0.1803	0.2358	0.2576	0.2363	0.1975	0.2535	0.2530	0.2713	0.2556	0.2542	0.2458	0.2404	0.2767
Fe^{3+}	0.1773	0.2040	0.1123	0.1739	0.1970	0.1627	0.1742	0.2244	0.2219	0.1582	0.1903	0.1949	0.2000	0.1768	0.1835
Fe^{2+}	1.2066	1.0528	1.2225	1.1705	1.1873	1.2188	1.2016	1.1083	1.1175	1.2125	1.1907	1.1585	1.1421	1.1775	1.1627
Mn	0.0167	0.0194	0.0214	0.0198	0.0181	0.0189	0.0221	0.0195	0.0171	0.0239	0.0165	0.0211	0.0214	0.0192	0.0170
Mg	1.1519	1.3385	1.3311	1.2418	1.1882	1.2472	1.2190	1.2331	1.1759	1.1679	1.1945	1.1855	1.2390	1.1715	1.1995
Ca	0.0026	0.0272	0.0157	0.0100	0.0014	0.0000	0.0077	0.0000	0.0063	0.0082	0.0065	0.0017	0.0071	0.0002	0.0000
Na	0.0117	0.0175	0.0619	0.0161	0.0145	0.0335	0.0137	0.0189	0.0143	0.0802	0.0280	0.0170	0.0116	0.0175	0.0132
K	0.9501	0.8734	0.9191	0.9024	0.8954	0.9096	0.8841	0.8761	0.8909	0.8975	0.8956	0.9135	0.8856	0.9356	0.9343
Total	7.8227	7.7960	7.8877	7.8261	7.8030	7.8373	7.8258	7.7756	7.7781	7.8418	7.8097	7.8051	7.8000	7.8232	7.8165
OH^-	2.0000	2.0000	2.0000	2.0000	2.0000	2.0000	2.0000	2.0000	2.0000	2.0000	2.0000	2.0000	2.0000	2.0000	2.0000
MF	0.4513	0.5119	0.4953	0.4765	0.4587	0.4711	0.4658	0.4769	0.4643	0.4558	0.4608	0.4631	0.4761	0.4603	0.4681
$Al^{VI} + Fe^{3+} + Ti$	0.4831	0.4672	0.3160	0.4654	0.4980	0.4093	0.4777	0.5196	0.5562	0.4515	0.4778	0.5079	0.4931	0.5017	0.4898
Fe^{2+} + Mn	1.2234	1.0722	1.2439	1.1903	1.2055	1.2377	1.2237	1.1278	1.1346	1.2365	1.2073	1.1796	1.1636	1.1967	1.1797
Ti/(Mg + Fe + Ti + Mn)	0.0922	0.0729	0.0629	0.0830	0.0904	0.0819	0.0702	0.0893	0.0908	0.0957	0.0898	0.0903	0.0863	0.0863	0.0975
Al/(Al + Mg + Fe + Ti + Mn + Si)	0.1888	0.1778	0.1740	0.1906	0.1883	0.1776	0.1964	0.1812	0.1920	0.1883	0.1845	0.1899	0.1868	0.1955	0.1890

Table 4. *Cont.*

Oxide	Samples													
	H-31	**H-32**	**H-33**	**H-34**	**H-35**	**H-36**	**H-37**	**H-38**	**H-39**	**H-40**	**H-41**	**H-42**	**H-43**	**H-44**
SiO_2	35.381	35.458	35.266	35.649	36.541	35.565	36.081	36.435	36.727	35.316	35.079	35.683	36.72	35.997
TiO_2	3.777	4.298	4.708	4.29	3.497	3.92	4.171	3.632	3.565	3.565	4.056	4.177	3.786	4.338
Al_2O_3	14.344	14.314	14.231	13.896	13.78	14.776	13.865	13.937	13.786	14.968	15.249	14.356	13.993	14.503
FeO	21.012	21.358	21.497	20.558	20.736	20.838	20.264	20.391	20.42	21.318	21.368	20.76	20.155	20.641
MnO	0.283	0.351	0.294	0.283	0.283	0.243	0.251	0.27	0.371	0.332	0.309	0.256	0.286	0.243
MgO	10.772	10.246	9.797	10.812	11.026	10.357	10.998	11.063	10.993	10.393	9.981	10.608	11.27	10.382
CaO	0.08	0.164	0.034	0.128	0.08	0.032	0.014	0.166	0.092	0.114	0.011	0	0.119	0
Na_2O	0.082	0.103	0.178	0.141	0.128	0.132	0.115	0.127	0.084	0.163	0.125	0.118	0.135	0.09
K_2O	9.372	8.816	9.124	9.383	9.07	9.317	9.36	9.187	9.293	9.082	9.186	9.367	8.946	9.311
Si	2.7443	2.7463	2.7389	2.7590	2.8164	2.7487	2.7832	2.8045	2.8236	2.7332	2.7131	2.7542	2.8101	2.7664
Al^{IV}	1.2557	1.2537	1.2611	1.2410	1.1836	1.2513	1.2168	1.1955	1.1764	1.2668	1.2869	1.2458	1.1899	1.2336
Al^{VI}	0.0556	0.0530	0.0415	0.0266	0.0681	0.0946	0.0437	0.0688	0.0728	0.0984	0.1032	0.0602	0.0722	0.0801
Ti	0.2204	0.2504	0.2751	0.2498	0.2028	0.2279	0.2421	0.2103	0.2062	0.2076	0.2360	0.2426	0.2180	0.2508
Fe^{3+}	0.1505	0.2068	0.1999	0.1688	0.1896	0.1804	0.1864	0.1864	0.1924	0.1628	0.1816	0.1798	0.2124	0.2109
Fe^{2+}	1.2125	1.1766	1.1964	1.1618	1.1471	1.1665	1.1209	1.1262	1.1205	1.2170	1.2006	1.1603	1.0775	1.1157
Mn	0.0186	0.0230	0.0193	0.0186	0.0185	0.0159	0.0164	0.0176	0.0242	0.0218	0.0202	0.0167	0.0185	0.0158
Mg	1.2456	1.1831	1.1343	1.2475	1.2669	1.1933	1.2647	1.2694	1.2599	1.1991	1.1508	1.2206	1.2857	1.1894
Ca	0.0066	0.0136	0.0028	0.0106	0.0066	0.0026	0.0012	0.0137	0.0076	0.0095	0.0009	0.0000	0.0098	0.0000
Na	0.0123	0.0155	0.0268	0.0212	0.0191	0.0198	0.0172	0.0190	0.0125	0.0245	0.0187	0.0177	0.0200	0.0134
K	0.9274	0.8711	0.9040	0.9264	0.8918	0.9186	0.9211	0.9021	0.9115	0.8967	0.9064	0.9224	0.8734	0.9129
Total	7.8495	7.7932	7.8001	7.8312	7.8104	7.8196	7.8136	7.8136	7.8076	7.8372	7.8184	7.8202	7.7876	7.7891
OH^-	2.0000	2.0000	2.0000	2.0000	2.0000	2.0000	2.0000	2.0000	2.0000	2.0000	2.0000	2.0000	2.0000	2.0000
MF	0.4741	0.4569	0.4448	0.4804	0.4832	0.4668	0.4886	0.4883	0.4851	0.4611	0.4507	0.4736	0.4956	0.4698
$Al^{VI} + Fe^{3+} + Ti$	0.4265	0.5103	0.5165	0.4452	0.4605	0.5029	0.4722	0.4656	0.4714	0.4688	0.5208	0.4825	0.5026	0.5418
Fe^{2+} + Mn	1.2311	1.1997	1.2157	1.1804	1.1655	1.1824	1.1373	1.1438	1.1447	1.2387	1.2208	1.1771	1.0961	1.1315
Ti/(Mg + Fe + Ti + Mn)	0.0774	0.0882	0.0974	0.0878	0.0718	0.0819	0.0855	0.0748	0.0736	0.0739	0.0846	0.0860	0.0775	0.0901
Al/(Al + Mg + Fe + Ti + Mn + Si)	0.1898	0.1892	0.1896	0.1841	0.1814	0.1956	0.1833	0.1834	0.1815	0.1974	0.2016	0.1898	0.1831	0.1914

The crystallization temperature of biotite is calculated as 500 °C~625 °C based on the temperature calculation formula of Ti and Mg/(Mg + Fe) contents in the biotite (Figure 6b). Moreover, there is a positive correlation between the total Al content of granodiorite and its consolidation pressure [56]; the formation pressure of biotite is calculated as 105.43~230.45 MPa (166.75 MPa in average) with the formula: P (kbar) = 3.03 × ^{T}Al−6.53 (±0.33), where ^{T}Al refers to the total number of Al cation in the biotite formula as calculated on a 22-oxygen-atom basis. The pressure then is converted to the emplacement depth by the formula: P = ρgD, where ρ = 2700 kg/m^3, g = 9.8 m/s^2, and the calculated crystallization depth of biotite was in the range of 3.98~8.71 km (6.3 km in average).

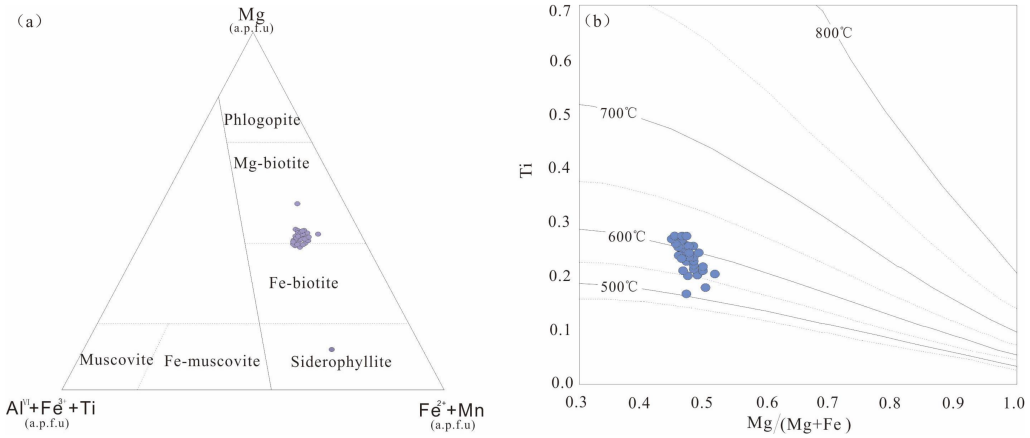

Figure 6. Classification diagram of biotite from the Zhouguan granodiorite (**a**) and Ti vs. Mg/(Mg + Fe) plot of biotite (**b**) (after Foster, 1960 [57]; Henry et al., 2005 [58]).

4.4. Amphibole Analysis Results

The main characteristics of amphibole in the Zhouguan granodiorite are as follows: The SiO_2 content is in the range of 42.27%~46.38%, and the MgO content is 10.44%~13.35%, which is obviously Mg-enriched (Table 5). The Al_2O_3 content is 5.79%~10.93%, FeO^T content is 14.46%~17.76%, and CaO content is 10.74%~111.51%. Therefore, the amphibole belongs to Ca-amphibole (Ca_a > 1.50), which can be further subdivided into magnesiohornblende, pargasite, and magnesiosadanagaite [59] (Figure 7).

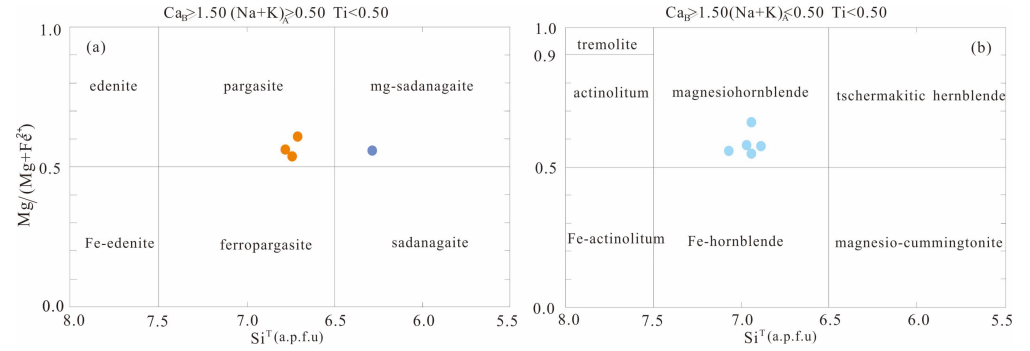

Figure 7. Classification of amphibole from the Zhouguan granodiorite [39].

The chemical composition of the amphibole is not only affected by the parental magma, but also related to the crystallization conditions (temperature, pressure, oxygen fugacity, and water content), so the composition of amphibole can be used to estimate the temperature and pressure conditions during crystallization in calc-alkaline magma. In this study, the crystallization pressures of the amphibole is calculated, using the formula [60–63]: P(kbar) = (−3.46 + 4.23Al^T); the formation pressure of amphibole is calculated to be 0.75~3.02 kbar and 4.64 kbar. These pressures can be converted to the crystallization

depth with the formula: P = ρgD, where ρ = 2700 kg/m^3, g = 9.8 m/s^2, and the calculated crystallization depth of amphibole is in the range of 2.81~11.4 km and 17.53 km.

The water content of magma has a positive correlation with oxygen fugacity [63]. According to the molecular formula of amphibole to calculate the water content of magma during crystallization, as corrected by Ridolfi (2009) [42], the calculated water content of the magma is in the range of 4.6%~5.6%, with an average of 5.1%, indicating that during this period, the magma has high water content.

Table 5. Composition of the amphiboles in Zhouguan granodiorite.

Component	Granodioriate								
	H-1	**H-2**	**H-3**	**H-4**	**H-5**	**H-6**	**H-7**	**H-8**	**H-9**
SiO_2	46.49	46.36	46.19	46.25	42.27	45.64	45.75	46.38	48.75
Al_2O_3	6.79	7.56	8.13	7.21	10.93	8.31	8.92	7.95	5.79
K_2O	0.62	0.56	0.72	0.83	1.22	0.72	0.63	0.72	0.62
P_2O_5	0.01	0.07	0.00	0.02	0.07	0.02	0.02	0.02	0.05
CaO	11.21	11.02	11.01	11.15	10.74	11.31	11.01	11.00	11.51
TiO_2	0.98	1.53	1.38	1.34	2.44	1.52	1.88	1.56	0.83
Cr_2O_3	0.02	0.03	0.02	0.00	0.07	0.00	0.01	0.07	0.00
MnO	0.55	0.38	0.41	0.55	0.49	0.42	0.43	0.42	0.48
FeO	16.75	14.46	16.19	17.76	17.31	16.48	14.88	15.73	17.13
Na_2O	1.23	1.81	1.70	1.45	1.97	1.74	1.98	1.82	1.21
MgO	11.72	13.35	11.62	11.23	10.44	11.81	12.55	12.78	12.23
Total	96.36	97.11	97.38	97.78	97.93	97.94	98.07	98.44	98.58
Based on 23 oxygen atoms and 16 cations, chemical analysis is based on (O + OH + F + Cl) = 24									
Si	6.93	6.79	6.82	6.85	6.28	6.72	6.67	6.73	7.11
Al^{IV}	1.07	1.21	1.18	1.15	1.72	1.28	1.33	1.27	0.89
Ti	0.00	0.00	0.00	0.00	0.00	0.00	0.00	0.00	0.00
T bit	8.00	8.00	8.00	8.00	8.00	8.00	8.00	8.00	8.00
Al^{VI}	0.13	0.10	0.24	0.10	0.20	0.16	0.20	0.09	0.10
Ti	0.11	0.17	0.15	0.15	0.27	0.17	0.21	0.17	0.09
Cr	0.00	0.00	0.00	0.00	0.01	0.00	0.00	0.01	0.00
Fe^{3+}	0.66	0.70	0.53	0.64	0.75	0.59	0.60	0.76	0.56
Mg	2.60	2.91	2.56	2.48	2.31	2.59	2.73	2.77	2.66
Fe^{2+}	1.43	1.07	1.47	1.56	1.40	1.44	1.21	1.15	1.53
Mn	0.07	0.05	0.05	0.07	0.06	0.05	0.05	0.05	0.06
C bit	5.00	5.00	5.00	5.00	5.00	5.00	5.00	5.00	5.00
Fe^{2+}	0.00	0.00	0.00	0.00	0.00	0.00	0.00	0.00	0.00
Ca	1.79	1.73	1.74	1.77	1.71	1.78	1.72	1.71	1.80
Na	0.21	0.27	0.26	0.23	0.29	0.22	0.28	0.29	0.20
B bit	2.00	2.00	2.00	2.00	2.00	2.00	2.00	2.00	2.00
Na	0.15	0.24	0.23	0.18	0.28	0.28	0.28	0.22	0.14
K	0.12	0.10	0.14	0.16	0.23	0.13	0.12	0.13	0.11
A bit	0.27	0.35	0.37	0.34	0.51	0.42	0.40	0.35	0.25
Si	6.93	6.79	6.82	6.85	6.28	6.72	6.67	6.73	7.11
$Mg/(Mg + Fe^{2+})$	0.65	0.73	0.63	0.61	0.62	0.64	0.69	0.71	0.63
Ca_B	1.79	1.73	1.74	1.77	1.71	1.78	1.72	1.71	1.80
$(Na + K)_A$	0.27	0.35	0.37	0.34	0.51	0.42	0.40	0.35	0.25
$(Ca + Na)_B$	2.00	2.00	2.00	2.00	2.00	2.00	2.00	2.00	2.00
Na_B	0.21	0.27	0.26	0.23	0.29	0.22	0.28	0.29	0.20
Ti	0.11	0.17	0.15	0.15	0.27	0.17	0.21	0.17	0.09
Al^T	1.19	1.31	1.41	1.26	1.91	1.44	1.53	1.36	0.99
Si*	8.31	8.07	8.11	8.23	7.50	7.99	7.88	8.05	8.52

4.5. Whole-Rock Sr-Nd Isotopes

The whole-rock Sr-Nd isotopic compositions are listed in Table 6. The results show that the ($^{87}Sr/^{86}Sr$) values range from 0.710424 to 0.711074, below the continental crustal average (0.717), and higher than the mantle average (0.709) [64], showing that it has the characteristics of A-type granite, which is similar to the magmatic rock in the basalt source area. The ($^{143}Nd/^{144}Nd$) values range from 0.511530 to 0.511808. The initial Sr-Nd isotopic ratios and the $\varepsilon_{Nd}(t)$ were calculated using the average crystallization age of 115 Ma. The Zhouguan granodiorite exhibit relatively homogeneous isotopic compositions, with $(^{87}Sr/^{86}Sr)_i$ = 0.709370–0.710619, $(^{143}Nd/^{144}Nd)_i$ = 0.511461–0.511726, and $\varepsilon_{Nd}(t)$ = −14.78−−19.95.

Table 6. Sr-Nd isotopic data of the Zhouguan granodiorite samples.

Samples	Rb (ppm)	Sr (ppm)	$^{87}Rb/^{86}Sr$	$^{87}Sr/^{86}Sr$	$\pm 2\sigma$	$(^{87}Sr/^{86}Sr)_i$	Sm (ppm)	Nd (ppm)	$^{147}Sm/^{144}Nd$	$^{143}Nd/^{144}Nd$	$\pm 2\sigma$	$(^{143}Nd/^{144}Nd)_i$	$\varepsilon_{Nd}(t)$	T_{DM} (Ma)	T_{2DM} (Ma)
PMZG0721-b1	222.8	1455.9	0.44	0.710424	0.000004	0.709669	8.87	60.20	0.088975	0.511605	0.000010	0.511535	−18.51	1885	3555
PMZG0721-b2	444.3	2343.7	0.55	0.710804	0.000003	0.709868	30.13	174.90	0.104086	0.511808	0.000008	0.511726	−14.78	1864	3106
PMZG0721-b8	149.3	1620.4	0.27	0.711074	0.000005	0.710619	7.60	52.53	0.087393	0.511530	0.000009	0.511461	−19.95	1951	3727
PMZG0721-b10	284.5	832.9	0.99	0.711055	0.000004	0.709370	5.99	40.40	0.089644	0.511600	0.000008	0.511530	−18.61	1901	3568

^{87}Rb decay $\lambda = 1.42 \times 10^{-11}$ year^{-1}; ^{147}Sm decay $K = 6.54 \times 10^{-12}$ year^{-1}; $\varepsilon_{Nd}(t)$ = were calculated with modern $(^{143}Nd/^{144}Nd)_{CHUR} = 0.512638$ and $(^{147}Sm/^{144}Nd)_{CHUR} = 0.1967$, and T_{DM} were calculated using present-day $(^{147}Sm/^{144}Nd)_{DM} = 0.2137$ and $(^{143}Nd/^{144}Nd)_{DM} = 0.51315$ [65].

5. Discussion

5.1. Age of Zhouguan Granodiorite

In recent years, with the advance and application of high-precision isotope dating technology, a lot of isotopic chronology studies on the Early Cretaceous granites in Jiaodong were performed [6,66–70]; however, the data on the ages of Zhouguan granodiorite are very few [71]. In this study, a systematic LA-MC-ICP-MS dating of the Zhouguan granodiorite was carried out and its age was determined as 115 Ma, which represents the emplacement time of the Zhouguan granodiorite.

Geologists adopted different isotope dating approaches to date the metallogenic age of the gold deposits in the area. These methods include the Ar-Ar method regarding the alterations in the sericite [65,72,73], the Ar-Ar method for muscovite and feldspar minerals associated with gold veins [72], the Ar-Ar and Rb-Sr methods for gold-bearing pyrite [74–77], and the SHRIMP U-Pb method [78–82] for hydrothermal zircon in gold-bearing quartz veins. The results show that the metallogenic ages of most gold deposits fall in the range of 115–122.5 Ma (Figure 8), although the types of deposits, their distribution area, and the geologic environments are slightly different. Therefore, most geologists generally believe that the large-scale gold mineralization event in the northwest Jiaodong area mainly occurred in 115 Ma ± 5 Ma, i.e., the late of the Early Cretaceous. The magmatic activity that produced the Zhouguan granodiorite during the same period may have an important influence on the formation of the gold deposits.

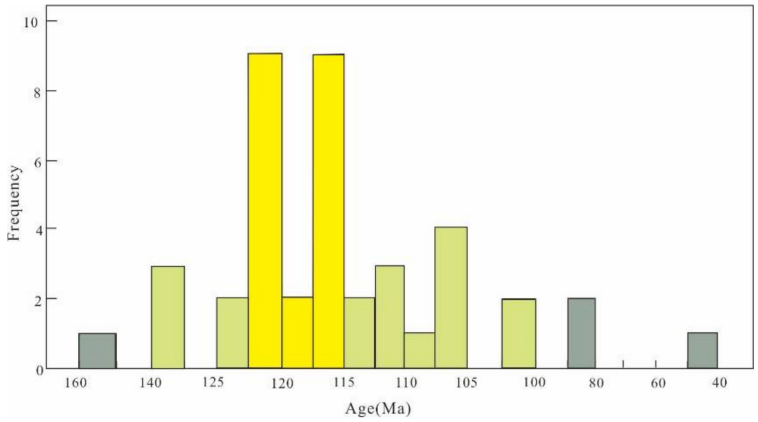

Figure 8. Metallogenetic age statistics of typical gold deposits in the Jiaodong area. (data from [72–78,83,84]).

5.2. Geochemical Features and Petrogenesis

The TAS and A/CNK-A/NK diagrams constructed from the results of whole-rock geochemical analysis show that the Zhouguan granodiorite belongs to the high-K calc-alkaline series and metaluminous to weakly peraluminous granitoids. The δEu value is in the range of 0.68~0.77, the moderately negative Eu anomaly indicates that plagioclase remained in the source area during the magmatic evolution, or indicates that it may be the result of fractional crystallization. Meanwhile, the low contents of HREE and Y suggest that amphibole/garnet may be present in the source area. The positive abnormalities in elements Nd and Hf demonstrate the typical geochemical characteristics of the high Ba-Sr granite, whereas the depletion of high-field strength elements (HFSE), such as Nb, Ta, and P shows its magmatic arc affinity. The Nb/Ta ratio is in the range of 16.6–21.9 (average 19.9), which is higher than the average ratio of the continental crust. The granodiorite has higher Sr and La contents but lower Y and Yb contents. In the Sr/Y-Y diagram (Figure 12c), all samples fall in the adakite area. The $FeO^T/(FeO^T + MgO)$-MgO diagram of biotite shows that the biotite has the characteristics of a crust–mantle mixed origin (Figure 9a). The TiO_2-FeO diagram of amphibole shows that the amphibole has two origins: the mantle origin and the crustal origin (Figure 9b).

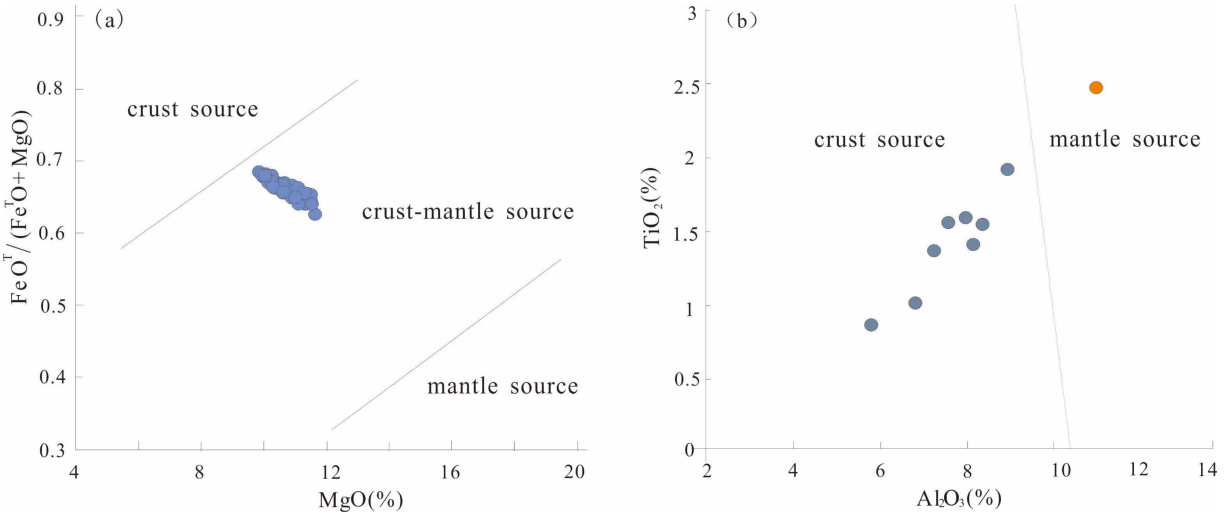

Figure 9. Diagram of Plot of $FeO^T/(FeO^T + MgO)$ vs. MgO from biotites (**a**) and diagram of TiO_2 vs. Al_2O_3 from amphiboles (**b**) (after Jiang and An, 1984 [79]; Zhou et al., 1986 [80]).

The Zhouguan granodiorites have high initial $^{87}Sr/^{86}Sr$ ratios (0.710424 to 0.711074) and negative $\varepsilon_{Nd}(t)$ values (−14.78–−19.95) (Figure 10a), indicating their origination of the continental crust [81,82]. The samples plot in the vicinity of Early–Middle Proterozoic crust and Archaean crust in the $\varepsilon_{Nd}(t)$ vs. T diagram, suggesting the source of Early–Middle Proterozoic and Archaean crusts (Figure 10b). The Sr and Nd isotopic compositions show that magmas originate from the lower crustal basement metamorphic rocks and lithospheric mantle melting [85].

Based on the synthesis of the whole-rock chemical analysis, single mineral EMPA analysis and the concept of the "trans-crustal magmatic system" [86], the Zhouguan granodiorite is considered to be a typical crust–mantle mixed origin granitoid in a continental magmatic arc environment. The forming process was that the magma of the mantle rose and mixed with the acid magma formed by the partial melting of the lower continental crustal rocks, and the mix magma crystallized in the upper crust to form Zhouguan granodiorite.

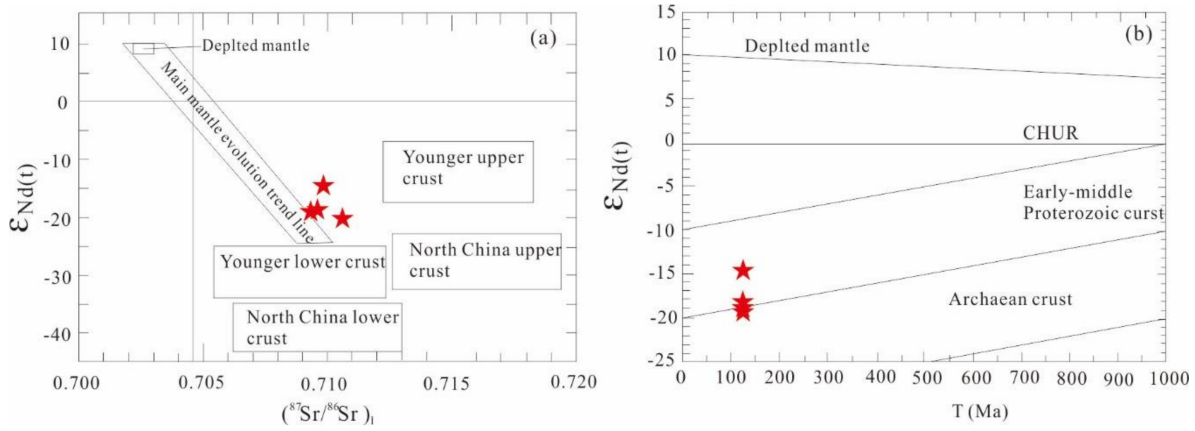

Figure 10. $(^{87}Sr/^{86}Sr)_i$ vs. $\varepsilon_{Nd}(t)$ isotope diagramand $\varepsilon_{Nd}(t)$ vs. T diagram of the Zhouguan granodiorite ((**a**) after Zhou et al., 2012 [87]; (**b**) after Jahn, 2000 [88]).

5.3. Significance of Amphibole and Biotite to Mineralization

A high oxygen fugacity of magma is required for the dissolution and migration of the Au element. Under a low oxygen fugacity environment, sulfur exists in the form of S^{2+}. During the crystallization process of magma, metal elements, such as Fe, Cu, Zn, and Au elements, etc, will form sulfides with S^{2+} to precipitate in magmatic rocks. Therefore, the

Au element is dispersed in the rock mass, which is not conducive to the enrichment and mineralization of gold [34]. Under a high oxygen fugacity environment, the S element exists in the form of SO_4^{2-}, which is beneficial to the migration and enrichment of the Au element in magma or fluid [42]. The high water content of magma, which has a positive correlation with oxygen fugacity, is another important factor when controlling the migration and enrichment of the Au element in gold deposits [33,64]. Water-rich magma can maximize the content of the Au element in the fluid, which is conducive for the Au element to migrate in the fluid [89].

In the biotite Fe^{3+}-Fe^{2+}-Mg diagram of the Zhouguan granodiorite (Figure 11a), all the data points are located between the two buffer lines of Ni-NiO and Fe_3O_4-Fe_2O_3, which indicates that the biotite was formed under a high oxygen fugacity condition; the amphibole Al^{IV}-Fe^{2+}/(Mg + Fe^{2+}) diagram shows that the amphibole was also formed under high oxygen fugacity conditions (Figure 11b), whose oxygen fugacity log f (O_2) is −11.82~−13.96. The water content ω (H_2O) of the magma is 4.62~5.43, with an average of 5.1%, indicating that the magma has a high water content. In summary, the parent magma forming the Zhouguan granodiorite has the characteristics of high oxygen fugacity and high water content, which is favorable for mineralization.

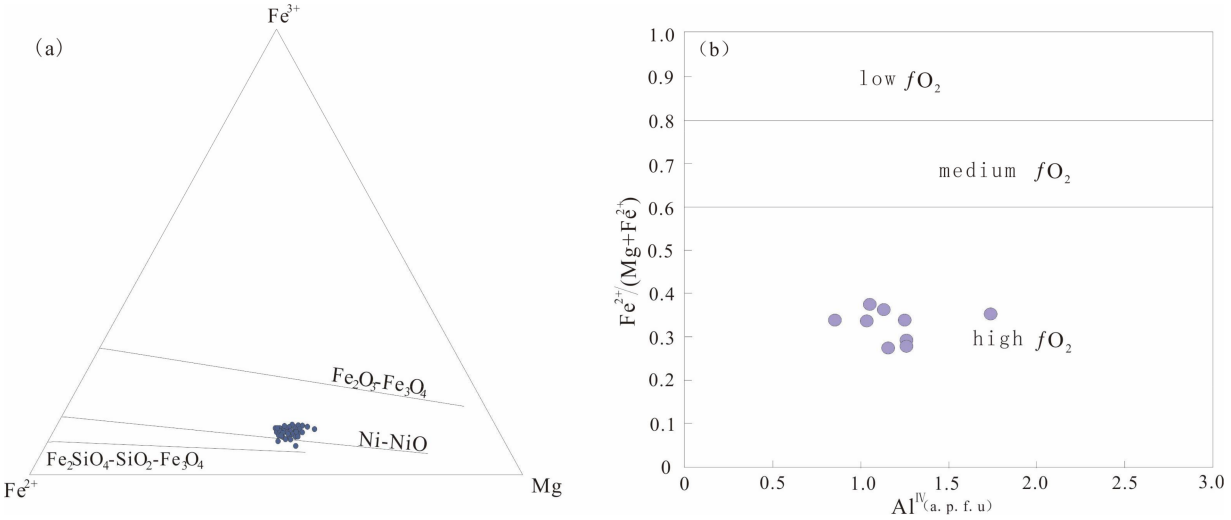

Figure 11. Plot of Fe^{3+}-Fe^{2+}-Mg for biotite (**a**) and Fe^{2+}/(Mg + Fe^{2+}) for amphibole (**b**) from the Zhouguan granodiorite (after Wones and Eugster, 1965 [36]; Dada, 2013 [90]).

5.4. Analysis of Petrogenetic Tectonic Environment in Relation to Metallogenic Model

The elements Rb, Y, and Nb in granitoids can be effectively used to distinguish between the granites formed in different tectonic environments, including volcanic arc granites, syn-collisional granites, intraplate granites, and ridge granites, etc. In the tectonic setting diagram of Y vs. Nb and Ta vs. Yb of granites (Figure 12a,b), the samples of Zhouguan granodiorite fall into the fields of volcanic arc granite and syn-collision granite. Combined with the analysis of the general plate movement environment, the Zhouguan granodiorite was formed in the extensional tectonic setting during the retreat of the Pacific plate, which belongs to the lithospheric extensional environment or the tectonic environment related to the gravitational collapse after collision orogeny.

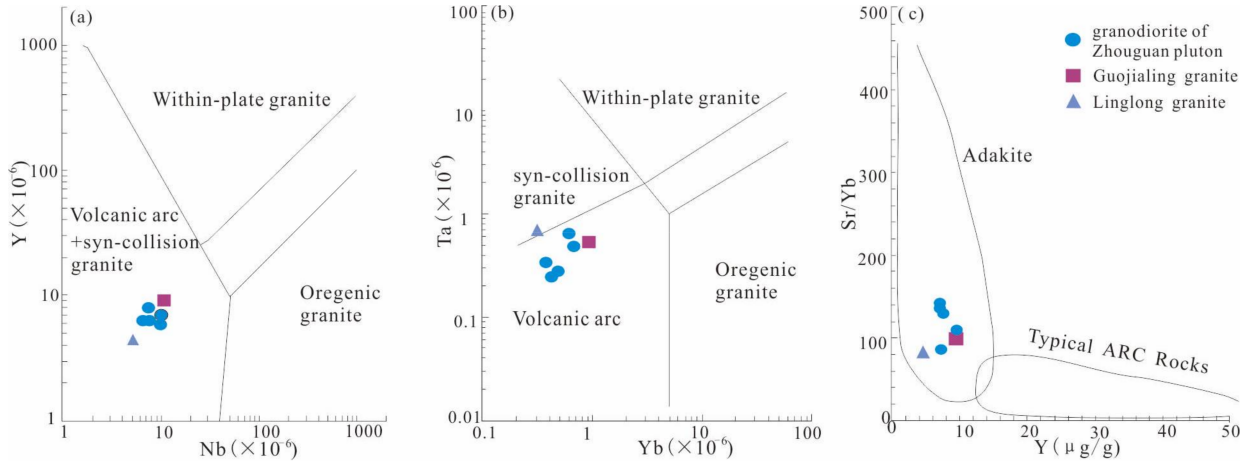

Figure 12. Diagrams of Y vs. tNb (**a**), Ta vs. Yb (**b**) and Sr/Yb vs. Y (**c**) for the Zhouguan granodiorite (after Pearce et al., 1984 [91]; Martin et al., 2005 [92]).

Based on the previous studies, and combined with the whole-rock and detailed single mineral analyses of the Zhouguan granodiorite, a model describing the formation of Zhouguan granodiorite is proposed. In the Early Cretaceous (125–135 Ma), the NW-trending compression caused by the subduction of the Pacific plate resulted in the destruction of the North China Craton [93–97]. A large-scale left-lateral strike-slip movement continued along the Tan-Lu fault zone. At the same time, a series of inherited secondary faults, which were formed by the same mechanism, were widely developed in the geological bodies on both sides of the Tan-Lu fault zone. These inherited secondary left-lateral strike-slip faults are characterized by small displacement, near vertical, and cutting Moho surfaces, whose name is short displacement cut-crust strike-slip fault [98].

During this period, the tectonomagmatic activity in the northwestern Jiaodong area was relatively weak, and the crust–mantle interaction was weak, too. A small amount of mantle-derived basic magma rose along the short displacement cut-crust strike-slip faults and formed basic dyke rocks at the shallow upper crust. The other partly mantle-derived basic magma was mixed with crust-derived magma to form intermediate acid magma, which then ascended and emplaced, forming the Guojialing granodiorites [86]. At this time, under the geodynamic background of intermedium acid magma intrusion and compression tensional movement of the plate, a series of shovel-type faults, such as the Jiaojia, the Sanshandao and the Zhaoping faults in NNE-trending faults occurred in the relatively weak lithological contact zones of the upper crust (0–5 km). Meanwhile, under the mechanical action of short displacement cut-crust strike-slip faults, a series of near-vertical faults, such as the Qixia, the Fengyi, the Yidao, and the Hulu Xian faults were formed; they are also the NNE-trending faults (Figure 13).

In the late of the Early Cretaceous (110–125 Ma), the tectonic environment changed from a compressional tectonic regime to an extensional tectonic system [98], and the front part of the Pacific subducting plate retreated, which resulted in the stretching, thinning, and damaging of the North China Craton. During the extensional thinning process of the North China Craton, the short displacement cut-crust strike-slip faults, which formed in the early stage, expanded and provided channels for the basic magma to rise. The rupture of the Moho caused a partial melting of the lithospheric mantle, producing basic magma. Part of the basic magma formed a series of dyke rocks during the intrusion of magma along near-vertical faults, such as lamprophyre, diorite porphyrite, etc. When the basic magma moved up to the lower crust, another part of the basic magma mixed with the magma from the partial melting of the lower crust, and formed the intermediate acid magma with high water content and high oxygenfugacity. The Zhouguan granodiorite was formed in the tectonic–magmatic system of this period (Figure 14).

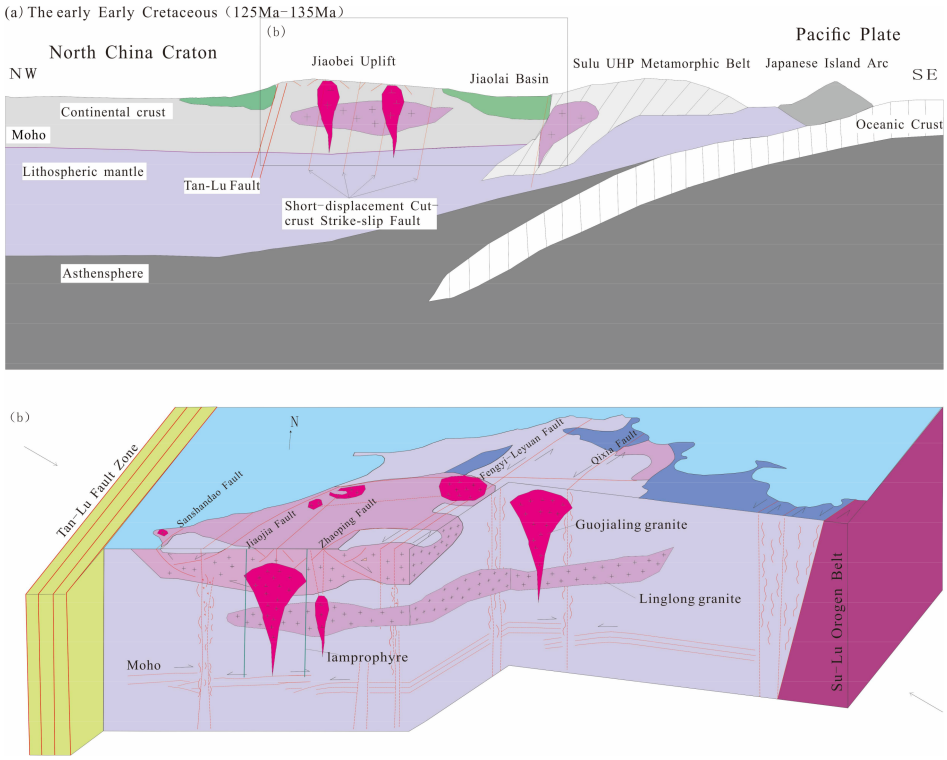

Figure 13. Geodynamic mechanism of magmatic activity (**a**) and diagram showing a structural pattern in Jiaodong (**b**) (after Song et al., 2020 [82]; Yu et al., 2018 [99]).

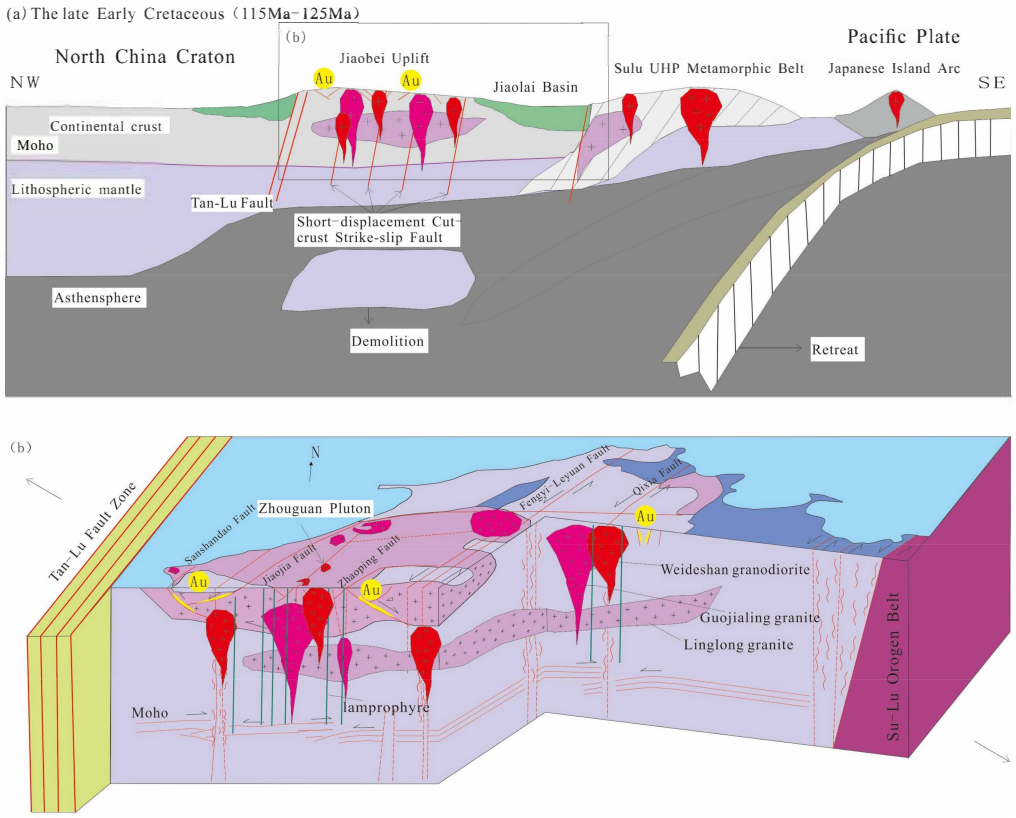

Figure 14. Geodynamic mechanism of magmatic activity (**a**) (after Song et al., 2020 [82]), diagram showing structural pattern in Jiaodong (**b**) (Yu et al., 2018 [99]).

6. Conclusions

(1) Through LA-MC-ICP-MS zircon U-Pb dating, the emplacement age of the Zhouguan granodiorite is determined as 115 Ma ± 0.77 Ma, indicating that the granodiorite occurred in the late of the Early Cretaceous.
(2) According to the petro-geochemical analysis, the Zhouguan granodiorite belongs to a high-K calc-alkaline series, metaluminous to weakly peraluminous granite, i.e., a typical crust–mantle mixed granitoids formed in a continental arc environment.
(3) According to an EPMA analysis of biotite and amphibole, the parent magma, which formed the Zhouguan granodiorite, is highly oxidized and hydrous, which is favorable for mineralization.
(4) Based on predecessors' research, and considering the development of short displacement cut-crust strike-slip faults and the trans-crustal magmatic system in the Jiaodong area, the petrogenesis of the formation model of the Zhouguan granodiorite in the area is proposed in this study.

Author Contributions: N.C., Z.H. and C.L. wrote the article. R.T., W.S., Y.X. (Yuqiang Xiong) and Z.L. revised the paper, conceived the experiments, and provided contributions to the data interpretation. The field work and preliminary study of samples were carried out by M.L. and X.W.; Y.X. (Yufeng Xie) conducted the geochemical analyses and reviewed both the science and English language. All authors have read and agreed to the published version of the manuscript.

Funding: This research was funded by the Natural Science Foundation of China with grant number of 42172094, the Natural Science Foundation Project of Shandong Province with grant number of ZR2019PD019, ZR2020QD029, ZR2020MD039.

Data Availability Statement: The data presented in this study are available in this paper.

Acknowledgments: The authors are grateful to Xie Yunhui and Wang Wenlu for their help during fieldwork, Shen kun, Shu Lei, Zhang Chenxi and Xu Jun for major and trace element analyses and U-Pb age. We acknowledge the efforts of anonymous reviewers, which significantly improved the manuscript.

Conflicts of Interest: The authors declare no conflict of interest.

References

1. Deng, J.; Wang, Q.F. Gold mineralization in China: Metallogenic provinces, deposit types and tectonic framework. *Gndwana Res.* **2016**, *36*, 219–274. [CrossRef]
2. Zhang, L.; Reberto, F.W.; Yang, L.Q.; David, I.G.; Sai, S.X.; Erin, M.; David, P.; Barry, P.M.; Liu, Y.; Deng, J. Mesozoic Orogenic Gold Mineralization in the Jiaodong Peninsula, China: A Focused Event at 120 ± 2 Ma During Cooling of Pregold Granit Intrusions. *Econ. Geol.* **2019**, *115*, 415–441. [CrossRef]
3. Song, M.C.; Lin, S.Y.; Yang, L.Q.; Song, Y.X.; Ding, Z.J.; Li, J.; Li, S.Y.; Zhou, M.L. Metallogenic model of Jiaodong Peninsula gold deposits. *Miner. Depos.* **2020**, *39*, 215–236.
4. Sang, L.K.; You, Z.D. Petrogenetic evolution of Linglong granites and their relationship to gold deposits in East Shandong Province. *Earth Sci.* **1992**, *17*, 521–529.
5. Wang, L.G.; Qiu, Y.M.; McNaughton, N.J.; Groves, D.I.; Luo, Z.K.; Huang, J.Z.; Miao, L.C.; Liu, Y.K. Constraints on crustal evolution and gold metallogeny in the northwestern Jiaodong Peninsula, China, from SHRIMP U-Pb zircon studies of granitoids. *Ore Geol. Rev.* **1998**, *13*, 275–291. [CrossRef]
6. Sun, H.S.; Sun, L.; Zhao, X.H.; Yang, K.C.; Cao, X.Z.; Liu, W.S.; Wang, C. Ore-controlling evidence and ore prospecting significance of Guojialing granodiorite in Northwest Jiaodong Peninsula. *Gold* **2007**, *28*, 14–18.
7. Yu, X.F.; Li, H.K.; Shan, W. Study on coupling between Yanshannian tectonic thermal events and gold mineralization in Jiaodong ore concentrating area in Shandong Province. *Acta Geol. Sin.* **2012**, *86*, 1946–1956.
8. Luo, Z.K.; Yang, X.Y.; Duan, L.A.; Sun, W.D. Geochemical and geochronological study of the gold-related Guojialing pluton and Shangzhuang pluton in Jiaobeiblock. *Acta Geol. Sin.* **2014**, *88*, 1874–1888.
9. Tian, J.P.; Tian, J.X.; Guo, R.P.; Wei, C.S.; Wang, L.G.; Yu, X.W.; Li, X.Z.; Huang, Y.B.; Zhang, C.C.; Liu, H.D.; et al. Jiaodong-type gold deposit related to crust source remelting layered granite and crust-mantle nixed granodiorite. *Acta Geol. Sin.* **2016**, *90*, 987–996.
10. Song, M.C.; Deng, J.; Yi, P.H.; Yang, L.Q.; Cui, S.X.; Xu, J.X.; Zhou, M.L.; Huang, T.L.; Song, G.Z.; Song, Y.X. The kiloton class Jiaojia gold deposit in eastern Shandong Province and its genesis. *Acta Geol. Sin.* **2014**, *88*, 801–824. [CrossRef]

11. Song, M.C.; Song, Y.X.; Li, J.; Li, S.Y. Metallogenic series of gold nonferrous metal deposits related to Cretaceous granites in eastern Shandong Peninsula, China. *Geotecton. Metallog.* **2015**, *39*, 828–843.
12. Li, J.W.; Bi, S.J.; Selby, D.; Chen, L.; Vasconcelos, P.; Thiede, D.; Zhou, M.F.; Zhao, X.F.; Li, Z.D.; Qiu, H.N. Giant Mesozoic gold provinces related to the destruction of the North China craton. *Earth Planet. Sci. Lett.* **2012**, *3490350*, 26–37. [CrossRef]
13. Zhang, S.H.; Zhao, Y.; Davis, G.A.; Ye, H.; Wu, F. Temporal and spatial variations of Mesozoic magmatism and deformation in the North Chian Craton: Implications for lithospheric thinning and decratonization. *Earth-Sci. Rev.* **2014**, *131*, 49–87. [CrossRef]
14. Zhao, R.; Wang, Q.F.; Deng, J.; Santosh, M.; Liu, X.F.; Cheng, H.Y. Late Mesozoic magmatism and sedimentation in the Jiaodong Peninsula: New constraints on lithospheric thinning of the North China Craton. *Lithos* **2018**, *322*, 312–324. [CrossRef]
15. Zhao, R.; Wang, Q.F.; Deng, J.; Santosh, M.; Liu, X.F.; Liang, Y.Y.; Cheng, H.Y. Characterizion episodic orogenesis and magmatism in eastern China based on detrital zircon from the Jiaolai Basin. *Am. J. Sci.* **2019**, *319*, 500–525. [CrossRef]
16. Yang, F.; Santosh, M.; Kim, S.W. Mesozoic magmatism in the eastern North China Craton: Insights on tectonic cycles associated with progressive craton destruction. *Gondwana Res.* **2018**, *60*, 153–178. [CrossRef]
17. Chen, Y.J.; Pirajno, F.; Qi, J.P. Origin of gold metallogeny and sources of ore-forming fluids, Jiaodong province, eastern China. *Int. Geol. Rev.* **2005**, *47*, 530–549. [CrossRef]
18. Zong, K.Q.; Liu, Y.S. Carbonate metasomatism in the lithospheric mantle: Implications for cratonic destruction in North China. *Sci. China Earth Sci.* **2018**, *61*, 711–729. [CrossRef]
19. Deng, J.; Yang, L.Q.; Li, R.H.; Groves, D.I.; Santosh, M.; Wang, Z.L.; Sai, S.X.; Wang, S.R. Regional structural control on the distribution of world-class gold deposits: An overview from the Giant Jiaodong Gold Province, China. *Geol. J.* **2019**, *54*, 378–391. [CrossRef]
20. Liang, Y.Y.; Deng, J.; Liu, X.F.; Wang, Q.F.; Ma, Y.; Gao, T.X.; Zhao, L.J. Water contents of Earth Cretaceous mafic dikes in the Jiaodong Peninsula, eastern North China Craton: Insights into an enriched lithospheric mantle source metasomatized by Paleo-Pacific plate subduction-related fluids. *J. Geol.* **2019**, *127*, 343–362. [CrossRef]
21. Wang, Q.F.; Zhao, H.S.; Groves, D.I.; Deng, J.; Zhang, Q.W.; Xue, S.C. The Jurassic Danba hypozonal orogenic gold deposit, western China: Indirect derivation from fertile mantle lithosphere metasomatized during Neoproterozoic subduction. *Miner. Depos.* **2020**, *55*, 309–324. [CrossRef]
22. Deng, J.; Liu, X.F.; Dilek, Y.; Liang, Y.Y. Isotopic characterization and petrogenetic modeling of Early Cretaceous mafic diking-Lithospheric extension in the North China Craton, eastern Asia. *GSA Bull.* **2017**, *129*, 1379–1407. [CrossRef]
23. Deng, J.; Wang, Q.F.; Santosh, M.; Liu, X.F.; Liang, Y.Y.; Yang, L.Q.; Zhao, R.; Yang, L. Remobilization of metasomatized mantle lithosphere: A new model for the Jiaodong gold province, eastern China. *Miner. Depos.* **2020**, *55*, 257–274. [CrossRef]
24. Liang, Y.Y.; Deng, J.; Liu, X.F.; Wang, Q.F.; Qin, C.; Li, Y.; Yang, Y.; Zhou, M.; Jiang, J.Y. Major and trace element, and Sr isotope compositions of clinopyroxene phenocrysts in mafic dykes on Jiaodong Peninsula, southeastern North China Craton: Insights into magma mixing and source metasomatism. *Lithos* **2018**, *302–303*, 480–495. [CrossRef]
25. Groves, D.I.; Santosh, M.; Deng, J.; Wang, Q.F.; Yang, L.Q.; Zhang, L. A holistic model for the origin of orogenic gold deposits and its implications for exploration. *Miner. Depos.* **2020**, *55*, 275–292. [CrossRef]
26. Wang, F.F.; Han, Z.Z.; Zhang, Y.; Lai, Z.Q.; Ai, L.N. Geochemical and petrogenesis of the Yashan granite and its enclaves, Qixia. *Contrib. Geol. Miner. Resour. Res.* **2019**, *34*, 393–405.
27. Xue, F.; Santosh, M.; Tsunogae, T.; Yang, F. Geochemical and isotopic imprints of early cretaceous mafic and felsic dyke suites track lithosphere-asthenosphere interaction and craton destruction in the North China Craton. *Lithos* **2019**, *326–327*, 174–199. [CrossRef]
28. Cui, T.S. Genetic mineralogy Research on hornblende of Shanzhang Guojialing granodiorite, Jiaodong. *J. Guilin Coll. Geol.* **1994**, *14*, 396–400.
29. Cui, T.S. Genetic Mineralgoy of Biotite from Guojialing Granodiorites. *Acta Petrol. Mineral.* **1995**, *14*, 179–184.
30. Lu, L.N.; Fan, H.R.; Hu, F.F.; Yang, K.F.; Lan, T.G. Emplacement depth of the Guojialing granodiorites from the northwestern Jiaodong Peninsula eastern China: Evidences from hornblende thermobarometry and fluid inclusions. *Acta Petrol. Sin.* **2011**, *27*, 1521–1532.
31. Du, J.G.; Shen, J.F.; Liu, C.; Liu, H.M. Study of Minerals in Congjia Granodioritic pluton and dioritic veins of Linglong ore field, eastern Shandong. *Miner. Pet.* **2014**, *34*, 40–47.
32. Sai, S.X.; Zhao, T.M.; Wang, Z.L.; Huang, S.Y.; Zhang, L. Petrogenesis of Linglong biotite granite: Constraints from mineralogical characteristics. *Acta Petrol. Sin.* **2016**, *32*, 2477–2493.
33. Yang, Y.; Wang, X.X.; Yu, X.W.; Ke, C.H.; Wang, L.M.; Guo, R.P.; Wang, S.A.; Li, X.X. Chemical composition of biotite and amphibole from Mesozoic granites in northwestern Jiaodong Peninsula, China, and their implications. *Acta Petrologica Sin.* **2017**, *33*, 3123–3136.
34. Chen, G.Y.; Sun, D.S.; Zhou, X.R.; Shao, W.; Gong, R.T.; Shao, Y. *Genetic Mineralogy and Gold Mineralization of Guojialing Granodiorite from Eastren Shandong China*; Beijing Publishing House of China University of Geolosciences: Beijing, China, 1993; pp. 1–130.
35. Li, H.L.; Bi, X.W.; Tu, G.Z.; Hu, R.Z.; Peng, J.T.; Wu, K.X. Mineral chemistry of biotite from Yanbeipluton: Implication for metallogeny. *Miner. Pet.* **2007**, *27*, 49–54.
36. Wones, D.R.; Eygster, H.P. Stability of biotite: Experment, theory, and application. *Am. Mineral.* **1965**, *50*, 1228–1272.
37. Butkhard, D.J.M. Temperature and redox path of biotite-bearing intrusives: A nethod of estimation applied to S- and I-type granites from Australia. *Earth Planet. Sci. Lett.* **1991**, *104*, 89–98. [CrossRef]

38. Kesler, S.E.; Issigonis, M.J.; Brownlow, A.H. Geochemistry of biotites from mineralized and barren intrusive systems. *Econ. Geol.* **1975**, *70*, 559–567. [CrossRef]
39. Hammarstrom, J.M.; Zen, E. Aluminum in hornblende: An empirical igneous geobarometer. *Am. Mineral.* **1986**, *71*, 1297–1313.
40. Chen, G.Y.; Sun, D.S.; Yin, H.A. *Genetic Mineralogy and Prospecting Mineralogy*; Chongqing Publishing House: Chongqing, China, 1988; pp. 555–647.
41. Zhou, Z.X. Application of chemical composition, trace elements, Ree, Cu, Cl, F, etc. of Mg, Fe mica in identifying petrogenetic types. In *Two types of Mesozoic porphyry deposits in Eastern China*; Wu, L., Li, B., Eds.; Science Press: Beijing, China, 1991; pp. 76–82.
42. Ridolfi, F.; Renzulli, A.; Puerini, M. Stability and chemical equilibrium of amphibole in calc-alkaline magmas: Au overview, new thermobarometric formulations and application to subduction-related volcanoes. *Contrib. Mineral. Petrol.* **2009**, *160*, 45–66. [CrossRef]
43. Zhang, Z.Q.; Zhang, C.J.; Wang, S.J.; Liu, S.C.; Wang, L.M.; Du, S.X.; Song, Z.Y.; Zhang, S.K.; Yang, E.X.; Cheng, G.S.; et al. View on classicication and Contrast of tectonic units in strata in Shandong Province. *Shandong Land RTsources* **2014**, *30*, 1–23.
44. Yang, L.Q.; Deng, J.; Wang, Z.L. Ore-controlling structural pattern of Jiaodong gold deposits: Geological-geophysical integration constraints. In *The Deep-Seated Strucutres of Earth in China*; Chen, Y.T., Jin, Z.M., Shi, Y.L., Eds.; Sciences Press: Beijing, China, 2014; pp. 1006–1030.
45. Martin, H. Theadakiticmagmas: Modern analogue of Archean granitoids. *Lithos* **1999**, *46*, 411–429. [CrossRef]
46. Smithes, R.H. The Archaeantonalite-trondhjemite-granodiorite(TTG) series is not an analogue of Cenozoic adakite. *Earth Planet. Sci. Lett.* **2000**, *182*, 115–125. [CrossRef]
47. Wang, Z.L.; Zhao, R.X.; Zhang, Q. Magma mixing for the high Ba-Sr Guojialing-type granitoids in Northwest Jiaodong Peninsula: Constraints from petrogeochemistry and Sr-Ndisotopes. *Acta Petrol. Sin.* **2015**, *30*, 2595–2608.
48. Song, S.G.; Niu, Y.L.; Wei, C.J. Metamorphism, anatexis, zircon ages and tectonic evolution of the Gongshan block inthe northern Indochina continent: An eastern extension of the Lhasa Block. *Lithos* **2010**, *120*, 327–346. [CrossRef]
49. Wang, Z.L.; Gong, Q.J.; Sun, X. LA-ICP-MSzircon U-Pb geochronology of quartz porphyry from the Niutougou gold deposit in Songxian County, Henan Province. *Acta Geol. Sin.* **2012**, *86*, 370–382.
50. Lin, W.W.; Peng, L.J. The estimation of Fe^{3+} and Fe^{2+} contents in amphibole and biotite from empa data. *J. Chang. Univ. Earth Sci.* **1994**, *24*, 155–162. [CrossRef]
51. Jacobsen, S.B.; Wasserburg, G.J. Sm-Nd isotopic evolution of chondrites. *Earth Planet. Sci. Lett.* **1980**, *50*, 139–155. [CrossRef]
52. Sun, S.S.; Mcdonough, W.F. Chemical and isotopic systematics of oceanic basalts: Implications for mantle composition and processes. In *Magmatism in the Ocean Basins*; Saunders, A.D., Norry, M.J., Eds.; Geological Society Special Publication: London, UK, 1989; pp. 313–345.
53. Foster, M.D. *Interpretation of the Composition of Trioctahedral Micas*; USGS: Reston, VA, USA, 1960; pp. 11–40.
54. Henry, D.J.; Guidotti, C.V.; Thomson, J.A. The Ti-saturation surface for low-to-medium pressure metapelitic biotites: Implications for geothermometry and Ti-substituton mechanisms. *Am. Mineral.* **2005**, *90*, 316–328. [CrossRef]
55. Stone, D. Temperature and pressure variations in suites of Archean felsic plutonic rocks, Berens river area, northwest superior province Ontario, Canada. *Can. Mineral.* **2000**, *38*, 455–470. [CrossRef]
56. Buddington, A.F.; Lindsley, D.H. Iron-titanium oxide minerals and synthetic equivalents. *J. Perrology* **1964**, *5*, 310–357. [CrossRef]
57. Albuquerque, C.A.R.D. Geochemistry of biotites from granitoids rocks, northern Portugal. *Geochim. Cosmochim. Acta* **1973**, *37*, 1779–1802. [CrossRef]
58. Uchida, E.; Endo, S.; Makino, M. Relationship between solidification depth of tranitic rocks and formation of hydrothermal ore deposits. *Resour. Geol.* **2007**, *57*, 47–56. [CrossRef]
59. Leake, B.E.; Woolley, A.R.; Arps, C.E.S. Nomenclature of amphiboles: Report of the Subcommittee on Amphiboles of the International Mineralogical Association, Commission on New Minerals and Mineral Names. *Can. Mineral.* **1997**, *35*, 219–246.
60. Hollister, L.S.; Grissom, G.C.; Peters, E.K.; Stowell, H.H. Confirmation of the empirical correlation of Al in hornblende with pressure of solidification of calc-alkaline plutons. *Am. Mineral.* **1987**, *72*, 231–239.
61. Johnson, M.C.; Rutherford, M.J. Experimental calibration of the aluminium in hornblende geobarometer with application to long valley caldera(California). *Volcan. Rocks* **1989**, *17*, 837–841.
62. Schmidet, M.W. Amphibole composition in tonalite as a function of pressure: Au experimental calibration of the Al-in-hornblende barometer. *Contrib. Mineral. Petrelogy* **1992**, *110*, 304–310. [CrossRef]
63. Ridolfi, F.; Puerini, M.; Renzuilli, A. The magmatic feeding system of El Reventador volcano (Sub-Andean zone, Ecuador) constrained by texture, mineralogy and thermobarometry of the 2002 erupted products. *J. Volcanol. Geotherm. Res.* **2008**, *176*, 94–106. [CrossRef]
64. Kelley, K.Y.; Cottrell, E. Water and the oxidation state of sub-duction zone magmas. *Science* **2009**, *325*, 605–607. [CrossRef]
65. Liu, Y.; Deng, J.; Wang, Z.L.; Zhang, L.; Liu, X.; Zheng, X.; Wang, X.; Zhang, C. Ziron U-Pb age, Lu-Hf isotopes and petrogeochemistry of the monzogranites from Xincheng gold deposit, northwestern Jiaodong Peninsula, China. *Acta Petrol. Sin.* **2014**, *30*, 2559–2573.
66. Zhu, R.X.; Chen, L.; Wu, F.Y.; Liu, J.L. Timing scale and mechanism of the destruction of the North China Craton. *Sci. China Earth Sci.* **2011**, *54*, 789–797. [CrossRef]
67. Xie, H.Q.; Wan, Y.S.; Wang, S.J.; Liu, D.Y.; Xie, S.W.; Liu, S.J.; Dong, C.Y.; Ma, M.Z. Geology and zircon dating of trondhjemitic gneiss and amphibolite in the Tangezhuang area, eastern Shandong. *Acta Petrol. Sin.* **2013**, *29*, 619–629.

68. Wang, S.J.; Wang, L.M.; Wan, Y.S.; Zhang, C.J.; Song, Z.Y.; Wang, J.G. Study on Intrusibe Rocks Forming Period and Stages Division in Ludong Area. *Shandong Land RTsources* **2009**, *25*, 8–22.
69. Ren, T.L.; Wang, L.M.; Zhu, X.Q.; Yu, X.W.; Yang, Z.Y.; Liu, H.D.; Guo, R.D.; Tao, Y.B. Early Cretaceous Weideshan Period Granite in Jiaodong Area. *Shandong Land RTsources* **2021**, *37*, 1–12.
70. Deng, J.; Fang, Y.; Zhou, X.Q. Inversion of ore-forming structural stress field and its ore-controlling effect in the gold ore zone in Northwest Jiaodong, Shandong. *Reg. Geol. China* **1995**, *3*, 253–260, (In Chinese with English abstract).
71. Li, H.M.; Mao, J.W.; Shen, Y.C. Ar-Ar Ages of K-feldspar and Quartz from Dongji Gold Deposit, Northwest Jiaodong, and Their Significance. *Miner. Depos.* **2003**, *1*, 72–77.
72. Luo, W.C.; Wu, Q.S. Using Altered Minerals to Determine the Metallogenic Age of Jiaodong Gold Deposit. *Chin. Sci. Bull.* **1987**, *16*, 1245–1248.
73. Li, H.Q.; Liu, J.Q.; Wei, L. *Chronology of Fluid Inclusions in Hydrothermal Deposits and Their Geological Applications*; Geological Publishing House: Beijing, China, 1993; pp. 1–126.
74. Mao, J.W.; Li, H.M.; Wang, Y.T. Hydrogen, oxygen, carbon and sulfur isotopic evidence for the involvement of mantle fluids in the mineralization of the Jiaodong gold deposit. *Acta Geol. Sin.* **2005**, *79*, 839–857.
75. Yang, J.H.; Zhou, X.H. Rb-Sr, Sm-Nd, and Pb isotope systematics of pyrite: Implications for the age and genesis of lode gold deposits. *Geology* **2001**, *29*, 711–714. [CrossRef]
76. Wang, Y.W.; Zhu, F.S.; Gong, R.T. Study on the Metallogenic Chronology of Gold Deposits in Jiaodong Gold Deposit Concentration Area. *Gold Geol.* **2002**, *8*, 48–55, (In Chinese with English abstract).
77. Chen, Y.-J.; Pirajno, F.; Lai, Y.; Li, C. Metallogenic time and tectonic setting of the Jiaodong gold province, eastern China. *Acta Petrol. Sin.* **2004**, *20*, 907–922.
78. Feng, K.; Fan, H.R.; Hu, F.-F.; Yang, K.F.; Liu, X.; Shangguan, Y.N.; Cai, Y.C.; Jiang, P. Involvement of anomalously As-Au-rich fluids in the mineralization of Heilan'gou gold deposit, Jiaodong, China: Evidence from trace element mapping and in-situ sulfur isotope composition. *J. Asian Earth Sci.* **2018**, *160*, 304–321. [CrossRef]
79. Jiang, C.Y.; An, S.Y. On Chemical Characteristics of calcic amphiboles from igneous rocsk and their petrogenesis significance. *Miner. Rock* **1984**, *1*, 1–9.
80. Zhou, Z.X. The origin of intrusive mass in fengshandong, Hubei Province. *Acta Petrol. Sin.* **1986**, *2*, 59–70.
81. He, X.H.; Liu, Y.S.; Zhao, Z.F. Inproved in situ Hf isotope ratio analysis of zircon using newly designed X skimmer cone and jet sample cone in combination with the addition of nitrogen by laser ablation multiple collector ICP-MS. *J. Anal. At. Spectrom.* **2012**, *27*, 1391–1399.
82. Song, Y.X.; Yu, X.F.; Li, D.P.; Gen, K.; Wei, P.F.; Zuo, X.M.; Wang, X.F. Petrogenesis of the Beijie pluton from thenorthwestern Jiaodong Peninsula: Constraints from zircon U-Pb age, petrogeochemistry and Sr-Nd-Pb isotopes. *Acta Petrol. Sin.* **2020**, *36*, 1477–1500. [CrossRef]
83. Zhang, L.; Weinberg, R.; Yang, L.; Groves, D.I.; Sai, S.-X.; Matchan, E.; Phillips, D.; Kohn, B.P.; Miggins, D.P.; Liu, Y.; et al. Mesozoic orogenic gold mineralization in the Jiaodong Peninsula, China: A focused event at 120±2 Ma during cooling of pregold granite intrusions. *Econ. Geol.* **2020**, *115*, 415–441. [CrossRef]
84. Feng, K.; Fan, H.; Groves, D.I.; Yang, K.-F.; Liu, X.; Cai, Y.-C.; Hu, F.-F. Geochronological and sulfur isotopic evidence for the genesis of the post-magmatic, deeply sourced, and anomalously gold-rich Daliuhang orogenic deposit, Jiaodong, China. *Miner. Depos.* **2020**, *55*, 293–308. [CrossRef]
85. Spark, R.S.J.; Annen, C.; Blundy, J.D.; Cashman, K.V.; Rust, A.C.; Jackson, M.D. Formation and dynamics of magma reservoirs. *Philos. Trans. R. Soc. A* **2019**, *377*, 2139. [CrossRef]
86. Xie, Y.H.; Shan, W.; Yu, X.F.; Chi, N.J.; Wang, F.Y.; Li, D.P.; Zhang, Y.; Li, X.W. Identification of clinopyroxene antecrysts in Cretaceous lamprophyre dykes from the Jiaodong Peninsula and their geological significance. *Acta Petrol. Sin.* **2021**, *37*, 2203–2233.
87. Zhou, Z.H.; Mao, J.W.; Lyckberg, P. Geochronology and isotopic geochemistry of the A-type granites from the Huanggang Sn-Fe deposit, southern Great Hinggan Range, NE China: Implication for their origin and tectonic setting. *J. Asian Earth Sci.* **2012**, *49*, 272–286. [CrossRef]
88. Jahn, B.M.; Wu, F.Y.; Chen, B. Massive granitoid generation in Central Asia: Nd isotope evidence and implication for continental growth in the Phanerozoic. *Episodes* **2011**, *23*, 82–92. [CrossRef]
89. Qiu, K.F.; Deng, J. Petmgenesis of granitoids in the Dewulu skarn copper deposit: Implications for the evolution of the Paleotethys ocean and mineralization in westen Qinling, China. *Ore Geol. Rev.* **2017**, *90*, 1078–1098. [CrossRef]
90. Dada, O.A. Application of amphibole chemistry in determining the petrogenesis of hornblende-biotite granites from Toro comples, north central, Nigeria. *Cont. J. Earth Sci.* **2013**, *8*, 1–11.
91. Pearce, J.A.; Harris, N.B.; Tiindle, A.G. Trace element discrimination diagrams for the tectonic interpretation of granitoids. *J. Petrol.* **1984**, *25*, 956–983. [CrossRef]
92. Martin, H.; Henney, P.J.; Rapp, R. An overview of adakite, tonalite-trondhjemite-granodiorite (TTG), and sanukitoid: Relationships and some implications for crustal evolution. *Lithos* **2005**, *79*, 1–24. [CrossRef]
93. Fowler, M.B.; Henney, P.J.; Darbyshire, D.F. Petrogenesis of high Ba-Sr granites: The Rogart pluton, Sutherland. *J. Geol. Soc.* **2001**, *158*, 521–534. [CrossRef]

94. Menzies, M.A.; Fan, W.M.; Zhang, M. Palaeozoic and Cenozoic lithoprobes and the loss of >120 km of Archaean lithosphere, Sino-Korean craton, China. In: Prichard HM, Alabaster T, Harris NBWand Neary CR. Magmatic Processes and Plate Tectonics. *Geol. Soc. Lond. Spec. Publ.* **1993**, *76*, 71–81. [CrossRef]
95. Gao, S.; Rudnick, R.L.; Carlson, R.W. Re-Os evidence for replacement of ancient mantle lithosphere beneath the North China Craton. *Earth Planet. Sci. Lett.* **2002**, *198*, 307–322. [CrossRef]
96. Xu, X.S.; Fan, Q.C.; O'Reilly, S.Y. U-Pb dating of zircons from quartz diorite and its enclaves at Tongguanshan in Anhui and its petrogenetic implication. *Chin. Sci. Bull.* **2004**, *49*, 2073–2082. [CrossRef]
97. Yang, K.F.; Fan, H.R.; Santosh, M. Reactivation of the Archean lower crust: Implications for zircon geochronology, elemental and Sr-Nd-Hf isotopic geochemistry of Late Mesozoic granitoids from northwestern Jiaodong terrane, the North China Craton. *Lithos* **2012**, *146–147*, 112–127. [CrossRef]
98. Zhai, M.G.; Liu, W.J.; Yang, J.H. Large-scale gold ore concentration area and large-scale mineralization in Jiaodong. *Sci. China (Ser. D)* **2001**, *31*, 545–552.
99. Yu, X.F.; Shan, W.; Xiong, Y.X.; Geng, K.; Sun, Y.Q.; Chi, N.J.; Guo, B.K.; Li, D.P.; Li, H.K.; Song, Y.X.; et al. Deep structural framework and genetic analysis of gold concentration areas in the Northwestern Jiaodong Peninsula, China: A new understanding based on high-resolution reflective seismic survey. *Acta Geol. Sin.* **2018**, *92*, 1823–1840. (English Edition) [CrossRef]